A top-down insular cortex circuit crucial for non-nociceptive fear learning

Junho Han,[1, 2] Boin Suh,[1, 2] and Jin-Hee Han[1, 2, *]

[1]Department of Biological Sciences

[2]KAIST Institute for the BioCentury, Korea Advanced Institute of Science and Technology, Daejeon 34141, South Korea

*Correspondence: han.jinhee@kaist.ac.kr

Abstract

Understanding how threats in environments drive fear memory formation is crucial to understanding how organisms adapt to changing environments and treat threat-related disorders such as PTSD. Despite decades of pioneering work using the Pavlovian conditioning model, our understanding has been limited because only one type (an electric shock) among diverse threats has been exclusively used. We developed a threat conditioning paradigm by utilizing a looming visual threat as an unconditioned stimulus (US) in mice and identified a distinct threat conditioning circuit. Parabrachial CGRP neurons were required for conditioning and memory retrieval. Their upstream neurons in the posterior insular cortex (pIC) responded to looming stimuli and projections of these neurons to the parabrachial nucleus induced aversive affective states and drove conditioning. But the pIC to PBN pathway was dispensable for foot-shock conditioning. Our findings provide insights into how a simple pattern of non-nociceptive visual stimuli can induce aversive states and drive fear memory formation.

Introduction

In a dynamically changing environment, animals must learn the sensory cues and environmental contexts associated with threats to avoid or properly respond to potentially dangerous situations in the future. This type of adaptive learning is essential for animals' survival. However, maladaptive fear memories are thought to be the root of a broad range of anxiety-related mental disorders, including post-traumatic stress disorder (PTSD). Therefore, understanding how threats drive the formation of fear memory is imperative to treat these disorders (*1*). For this purpose, the Pavlovian fear conditioning paradigm (*2, 3*) has been extensively used as a model system across diverse animal species, especially in rodents, in which an initially neutral sensory stimulus such as an auditory sound, the conditioned stimulus (CS), is paired with an aversive stimulus such as an electric foot-shock, the unconditioned stimulus (US). As a result of learning, re-exposure to the CS induces fear-related behavioral responses such as freezing. This behavior model has greatly advanced our understanding of how fear memory is formed in the brain (*4–8*). Despite these advancements, our understanding has been limited because only one type (an electric foot-shock) among diverse threats has been used in most studies.

Pain is thought to be a critical driving factor for fear memory formation. Pain can be categorized into two dimensions: sensory pain and affective pain (*9–11*). Sensory pain encompasses the intensity, type, and location of physically perceived pain, whereas affective pain is defined as a feeling of unpleasantness (*9, 11–13*). This unpleasantness drives the desire to avoid aversive stimuli, thereby facilitating fear learning. Moreover, affective pain alone, in the absence of nociceptive stimuli, can induce PTSD (*14, 15*); for instance, media exposure to tragic events can lead to PTSD (*16, 17*). A nociceptive electric shock has been routinely used as a US in threat conditioning studies and it is well established that nociceptive stimuli such as electric shock are highly effective in driving fear memory formation. However, not all sensory stimuli that are aversive to animals and induce strong fear-related defensive behavioral responses are nociceptive. For instance, visual or chemical signals associated with predators can trigger strong fear-related behaviors such as freezing and running for escape. Although not nociceptive, these stimuli may induce aversive affective states in animals exposed to them and thereby drive fear learning and memory formation. This possibility, however, has been scarcely explored and existing results are inconsistent (*18–21*).

Conventionally, nociceptive US pathways in fear learning have been identified using foot-shock stimuli (*8, 22–25*). Among them, the thalamus and parabrachial nucleus (PBN) in the brainstem are recognized as major ascending nociceptive US pathways. The thalamus distributes nociceptive information widely across the brain (*26*), including the anterior cingulate cortex (ACC), prefrontal cortex, and amygdala, which are critical for fear learning (*27–30*). Thus, the thalamus has long been considered a central region in US pathways. In addition to this, recent evidence identified the PBN as another US pathway essential for fear learning by transmitting pain information to the central nucleus of the amygdala (CeA) and likely some other downstream areas. A previous study pinpointed that calcitonin gene-related peptide (CGRP)+ neurons in the PBN ($CGRP^{PBN}$ neurons) are essential for shock-induced threat conditioning in mice, and optogenetic activation of the $CGRP^{PBN}$ neurons to the CeA pathway induces fear learning (*31*). Based on anatomical connectivity, the spinal cord and dorsal periaqueductal gray (PAG) have been considered potential upstream areas relaying nociceptive information to the PBN (*32–34*). Interestingly, it has been shown that $CGRP^{PBN}$ neurons respond not only to electric shock but also to diverse non-nociceptive stimuli including a visual threat stimulus, raising the

possibility that these neurons may also be involved in fear learning by non-nociceptive stimuli (*35,36*).

Neural circuits for non-nociceptive US have been studied by using psychological stressors instead of foot-shock. Live cats or predator odors elicit strong innate fear responses in rodents and can lead to the formation of auditory and contextual fear memories (*37, 38*). Early lesion studies showed that regions such as the basolateral amygdala (BLA) (*39*) and ventral hippocampus (vHPC) (*40*), which are involved in shock conditioning, are also required for predator odor-induced fear learning. Additionally, the medial amygdala (MeA) (*41*), which is not involved in shock conditioning, was identified as a novel component of the fear learning in this context. Recent research using muscimol inactivation indicates that the posterior insular cortex (pIC) is crucial for both the formation and recall of predator odor-induced contextual fear memories (*42*) The insular cortex has been associated with processing negative emotions and cognitive information related to fear, anxiety, and disgust (*11, 43*). Animal studies have demonstrated that optogenetic activation of pIC induces an aversive state in mice (*44*) and insular cortex activity is crucial for the maintenance of learned fear (*45*). In humans, the affective and social pain correlates with activity in the ACC and insular (*11, 46, 47*). Also, in a fear learning using aversive pictures as US, the insular cortex shows increased activation when exposed to both the aversive picture and the CS (*48, 49*). Moreover, lesions in the insular cortex can result in pain asymbolia (*50*), where pain sensation is present but the unpleasantness is not perceived. These findings suggest that the insular cortex plays a crucial role in representing negative emotions and affect rather than processing somatosensory information related to nociception. Notably, the insular cortex has substantial reciprocal connections with the PBN (*51, 52*). The insular cortex may convey affective information to the PBN. Despite these findings, however, it is poorly understood how sensory signals with no nociceptive information produce aversive affective states and may drive fear memory formation. Particularly, little is known about neuronal circuit pathways engaged to mediate these functions.

While previous studies have used live cats and predator odors as non-nociceptive US stimuli in rodent fear learning models (*37, 38*), these models have significant limitations. The intensity and timing of odor stimuli are difficult to control precisely. Moreover, the effectiveness of fear learning varies with different predator odors (*38, 53*), which activate different brain regions (*20*). These complex chemosignals complicate the study of specific neural circuits in fear learning. In contrast, visual stimuli allow for precise experimental manipulation and effective observation of immediate animal responses. It has been reported that rapidly looming visual stimuli can trigger immediate defensive behaviors across various species, including rodents (*54, 55*), frogs (*56*), fishes (*57, 58*), primates (*59*), and humans (*60, 61*). An earlier pioneering work has established a visual threat model in mice by using a rapidly looming dark disc overhead mimicking fast-approaching motion of aerial predators (*54*).

Here, we developed a novel threat conditioning paradigm in mice by utilizing the previously developed looming visual threat. We discovered a distinct pIC-to-PBN circuit pathway that is sufficient to produce aversive affective states and threat conditioning but dispensable for foot-shock conditioning, highlighting its role in processing threat-relevant non-nociceptive visual information separate from sensory pain.

Results

Looming visual stimuli can drive threat conditioning as a US

We aimed to develop a threat conditioning model using a looming visual stimulus as a US. In this study, we used a rapidly expanding dark disc from overhead, increasing from 5 to 35 degrees of visual angle in 300 ms and remaining at that size for 500 ms, as a looming visual stimulus. Before investigating the visual threat learning, we first confirmed that this looming visual stimulus induces innate defensive responses in mice. When exposed to the 10 consecutive looming stimuli, mice immediately displayed a strong freezing response (**fig. S1, A to C**). However, there was little or no escaping behavior likely due to the lack of shelter in our test condition as reported previously (*62*). To determine the habituation to the stimulus, the same test was repeated across 5 days and we found no significant habituation to the looming stimulus (**fig. S1D**). Habituation could occur if the looming stimulus was repeatedly presented with a short time interval. To test this, a session of 5 consecutive looming stimuli was presented 10 times to mice with a 120-s intersession interval. Indeed, we observed a trend toward habituation to the looming stimulus over repeated exposures. Mice exhibited significant freezing responses until the 5th exposure but afterward, response began to be reduced, indicating a habituation effect (**fig. S1, E and F**). Based on these results, we decided to use five pairings of CS-US in the following conditioning experiments.

To investigate whether the looming visual stimuli can drive threat conditioning as a US, we paired a neutral auditory sound (2.7 kHz, 80 dB) as a CS with five consecutive looming stimuli as a US (hereafter, looming US). In the paired group, the tone was presented for 20 s with the last 4-s overlapped with the looming US. The CS and US were paired five times. In the unpaired group, basically the same CS and US were used but the only difference is they were unpaired; the looming US was presented first, followed by the tone presentation with a random interval of 15 to 30 s (**Fig. 1A**). The next day, mice were placed in a shifted context and tested for auditory fear memory. The mice only in the paired group, but not in the unpaired group, exhibited significant freezing response to the tone compared to the pre-CS period (**Fig. 1B**). On the following day, contextual fear memory was assessed by re-exposing mice to the conditioning chamber where they received the looming US. Both paired and unpaired groups showed significant freezing response (**Fig. 1C**). In an additional experiment, we tested a different number of CS-US pairings and found that a smaller number of pairings was not effective in driving threat conditioning (**Fig. 1, D and E**). Together, these results establish a threat conditioning by using a non-nociceptive visual threat as a US in mice. We used this model for threat conditioning in all the following experiments unless otherwise noted.

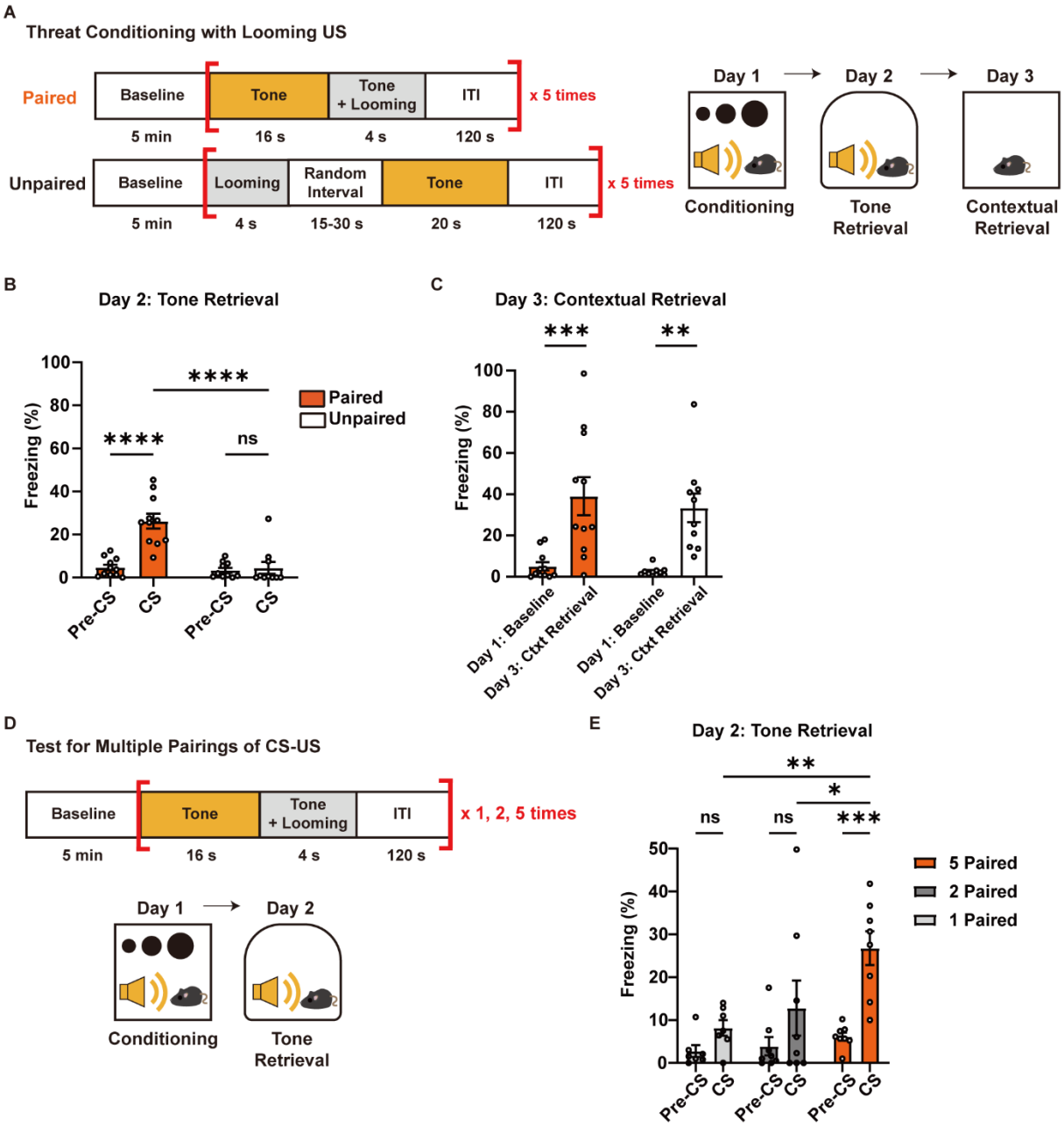

Fig. 1. Looming visual stimuli drive formation of auditory and contextual fear memory in mice

(**A**) Schematic of a threat conditioning protocol with looming visual stimuli. (**B**) Auditory fear memory was formed only in the paired group (Paired group, N= 11; Unpaired group, N= 10; RM two-way ANOVA, Time × Group, $F_{1,19}$= 17.2, P= 0.0005). (**C**) Both paired and unpaired groups show elevated levels of contextual freezing during re-exposure to the conditioning chamber on day3 (Paired group, N= 11; Unpaired group, N= 10; RM two-way ANOVA, Time × Group, $F_{1,19}$= 36.38, P< 0.0001). (**D**) Schematic of threat conditioning with different times of CS-US pairing (1, 2, and 5 times, respectively). (**E**) Single and double pairings of tone CS and looming US were not effective in driving the formation of auditory fear memory (Single-paired group, N= 7; Double-paired group, N= 8; Five-times paired group, N= 8; RM two-way ANOVA, Group, $F_{2,20}$= 4.500, P= 0.0243). All data are mean ± s.e.m. *p < 0.05. **p < 0.01. ***p < 0.001. ****p < 0.0001. ns, not significant.

178 **CGRP^{PBN} neurons are required for fear memory formation and its retrieval, but not**
179 **for innate defensive response to a visual threat**

180 Given the CGRP^{PBN} neurons are critical for the threat conditioning by a foot-shock, and
181 they also respond to looming visual stimuli in addition to many other aversive stimuli, we
182 reasoned that the CGRP^{PBN} neurons may also be involved in the formation of fear memory
183 by a visual threat. To test this, we inactivated synaptic transmission specifically in the
184 CGRP^{PBN} neurons by using the tetanus toxin light chain (TetTox). To specifically target
185 the CGRP^{PBN} neurons, Cre-dependent adeno-associated virus (AAV) encoding both
186 TetTox and dTomato was injected into the PBN of *Calca^{Cre}* transgenic mice, in which Cre
187 recombinase is specifically expressed in CGRP+ neurons (*63, 64*). The tdTomato alone
188 expression was used as a control. Two weeks after the viral injection, we performed
189 behavior experiments (**Fig. 2A**). Post hoc histological analysis confirmed highly restricted
190 viral expressions in the PBN (**Fig. 2B**). To examine whether the basal locomotor activity
191 and anxiety are normal, mice from both groups were subjected to an open-field test prior
192 to threat conditioning experiments and showed no significant differences in locomotor
193 activity and anxiety level (**Fig. 2C**). On the following days, these mice were trained for
194 threat conditioning with the looming US and tested for fear memory. During the
195 conditioning, mice from both control and TetTox groups showed increased freezing
196 response to the looming US with no group difference (measured during the first CS-US
197 pairing), suggesting that the CGRP^{PBN} neurons are not required for the innate defensive
198 response to the visual threat (**Fig. 2D**) consistent with a previous report (*36*). This result
199 was further confirmed by a separate experiment (**fig. S2, A and B**). Interestingly,
200 however, we found that the CGRP^{PBN} neurons were required for fear memory formation.
201 During fear memory tests, the mice in the TetTox group showed no significant increase in
202 freezing to the conditioned tone and context compared to the pre-CS period, while the
203 mice in the control group showed increased freezing (**Fig. 2, E and F**). These results
204 indicate that for a visual threat, although not required for innate response, the CGRP^{PBN}
205 neurons are involved in threat conditioning, suggesting a specific role for processing
206 learning signals rather than mediating reflective actions.

207 To further characterize the role of the CGRP^{PBN} neurons for threat conditioning by a
208 visual threat, we next employed optogenetic approaches. Cre-dependent AAV virus
209 encoding eNpHR3.0 fused with EYFP or EYFP alone was injected into the PBN of
210 *Calca^{Cre}* mice and optic fiber was placed right above the virus injection sites. The
211 CGRP^{PBN} neurons were inactivated by light illumination specifically during the
212 conditioning period starting from the onset of the first US presentation (**Fig. 2G**). Post hoc
213 histological analysis confirmed highly restricted eNpHR3.0 expressions in the PBN (**Fig.**
214 **2H**). As in the TetTox experiment, the immediate freezing response (measured during the
215 first CS-US pairing) was not affected (**Fig. 2I**). However, we observed no fear memory
216 formation in the eNpHR3.0 group compared to the control group, indicating that the
217 activity of CGRP^{PBN} neurons is required during conditioning for fear memory formation
218 (**Fig. 2J**). In a separate experiment, the CGRP^{PBN} neurons were inactivated specifically
219 during the retrieval test instead of conditioning (**Fig. 2K**). The mice in the eNpHR3.0
220 group, not in the control group, showed no significant increase in freezing to the tone CS,
221 indicating impaired memory retrieval (**Fig. 2L**). Taken together, our results demonstrate
222 that for a visual threat, the activity of the CGRP^{PBN} neurons is required not only for fear
223 memory formation but also for its retrieval, but not for innate behavioral response.

224

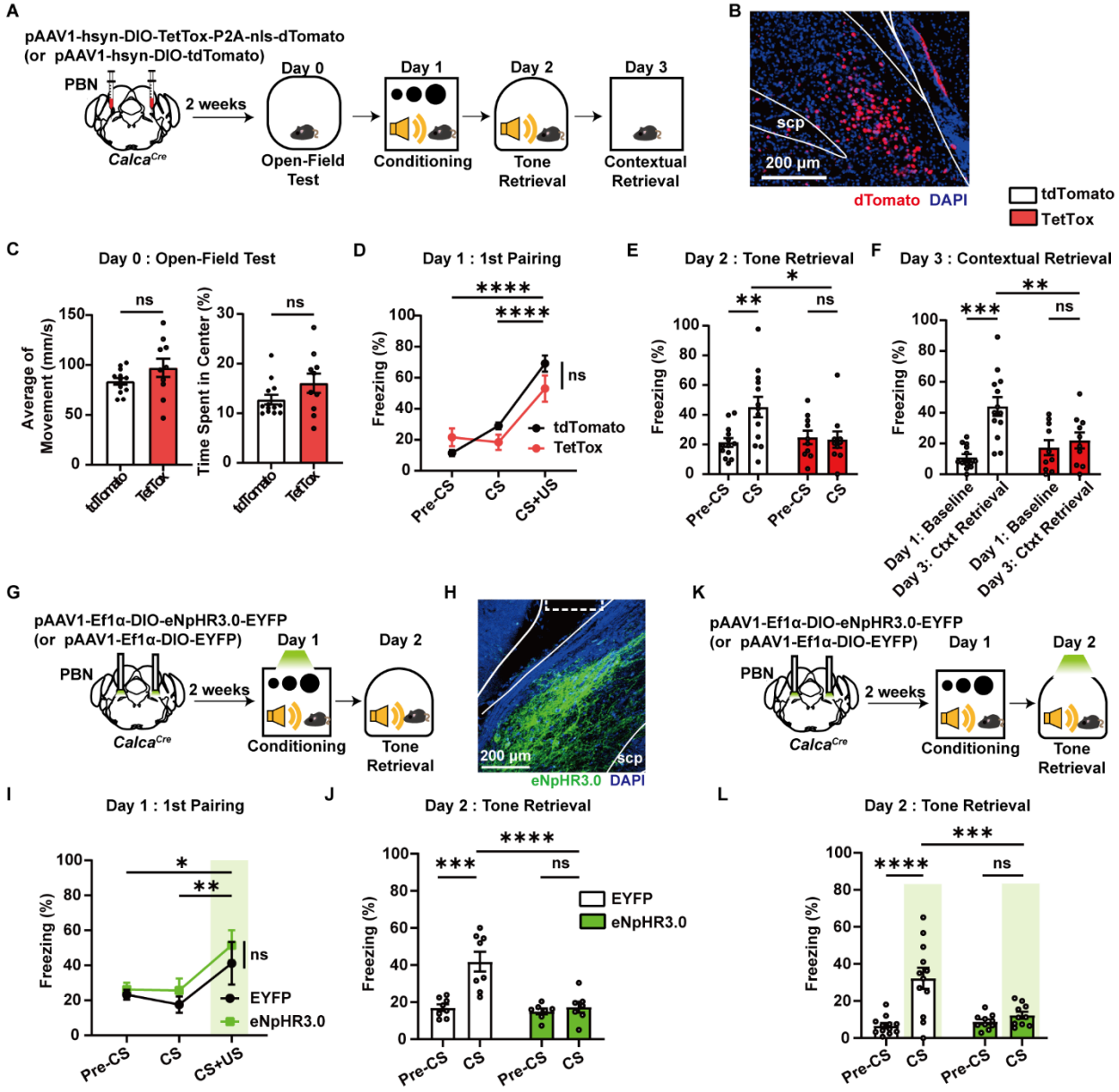

Fig. 2. The inhibition of CGRP^{PBN} neurons impairs formation and retrieval of fear memory, but not innate defensive behavior for looming visual stimuli

(**A**) Schematic of TetTox-mediated inhibition of CGRP^{PBN} neurons during visual US threat conditioning. (**B**) Representative image of a coronal section showing the expression of dTomato in the PBN, especially in the external lateral subdivision of PBN (PBel). Scale bars, 200 μm. SCP, superior cerebellar peduncle. (**C**) Average of movement (left; TetTox, N= 10; tdTomato, N = 13; two-tailed unpaired t-test, t_{21}= 1.518, P= 0.1439) and the time spent in the center zone (right, two-tailed Mann Whitney test, U= 46, P= 0.2569) were comparable between TetTox and tdTomato group. (**D**) Freezing levels during the first pairing of tone CS and looming US on Day 1 (RM two-way ANOVA, Time × Group, $F_{2,42}$= 5.334, P< 0.0086). (**E**) TetTox inhibition of CGRP^{PBN} neurons impairs auditory fear memory (RM two-way ANOVA, Time × Group, $F_{1,21}$= 7.251, P< 0.0136). (**F**) Contextual fear memory was impaired in the TetTox inhibition group (RM two-way ANOVA, Time × Group, $F_{1,21}$= 7.798, P< 0.0109). (**G**) Schematic of optogenetic inhibition of CGRP^{PBN} neurons during visual US conditioning. (**H**) Representative image of a coronal section showing the expression of eNpHR3.0-EYFP in CGRP^{PBN} neurons. The dotted rectangle indicates the location of the optic fiber tip. Scale bars, 200 μm. (**I**) Freezing levels

during the first pairing of tone CS and looming US on Day 1 (eNpHR3.0, N= 7; EYFP, N = 8; RM two-way ANOVA, Time, $F_{2,26}$= 7.167, P< 0.0033). (**J**) Inhibition of CGRP^{PBN} neurons during visual US conditioning impaired the formation of auditory fear memory (eNpHR3.0, N= 7; EYFP, N= 8; RM two-way ANOVA, Time × Group, $F_{1,13}$= 9.965, P< 0.0076). (**K**) Schematic of optogenetic inhibition of CGRP^{PBN} neurons during auditory memory retrieval. (**L**) Inhibition of CGRP^{PBN} neurons impaired retrieval of auditory fear memory (eNpHR3.0, N = 10; EYFP, N = 12; RM two-way ANOVA, Time × Group, $F_{1,20}$= 18.16, P< 0.0004). All data are mean ± s.e.m. *p < 0.05. **p < 0.01. ***p < 0.001. ****p < 0.0001. ns, not significant.

One possible interpretation of these results is that as a consequence of conditioning, the initially neutral tone might acquire an ability to activate the CGRP^{PBN} neurons likely by synaptic plasticity-dependent mechanisms, and thereby induce freezing, a conditioned response. This could be a mechanism by which the neutral tone is transformed into an aversive signal through the conditioning process. Consistently, it has been previously shown that an aversive intense sound stimulus activates the CGRP^{PBN} neurons and such activation is required for freezing induced by the sound (*36*). To test this idea, we performed in vivo fiber photometry calcium recordings to monitor the responses of the CGRP^{PBN} neuronal populations to the tone before and after conditioning. Cre-dependent AAV virus encoding GCaMP6m calcium indicator was injected into the PBN of *Calca*^{Cre} mice and optic fiber was placed right above the viral injection sites (**fig. S3, A and B**). During conditioning, the CGRP^{PBN} neurons showed increased calcium responses to the looming US (**fig. S3, C, D, and F**), consistent with a previous study (*36*). Initially, the CGRP^{PBN} neurons showed no significant calcium response to the tone CS (measured during the first CS-US pairing) **(fig. S3, C and G)**, but afterward, a slight increase was observed as the pairing was repeated, especially just before the onset of the looming US (**fig. S3, D and H**). The next day after the conditioning, the CGRP^{PBN} neurons showed significantly increased calcium response to the tone (**fig. S3, E and I**). These recording results support the idea that the increased response of the CGRP^{PBN} neurons to the tone CS is a potential mechanism underlying threat conditioning by a visual threat.

pIC and SC cells projecting to the CGRP^{PBN} neurons are activated by looming visual stimuli

Given the involvement of CGRP^{PBN} neurons in the threat conditioning by a visual threat, we next asked which brain areas convey non-nociceptive US information to the CGRP^{PBN} neurons for threat conditioning. In the case of nociceptive stimuli, the spinal cord or dorsal PAG has been suggested as a potential upstream area relaying nociceptive information to the PBN (*31–34*). However, it has been unclear for non-nociceptive stimuli. So, we searched for the inputs that are required for activation of the CGRP^{PBN} neurons in response to looming visual stimuli. We set out by performing brain-wide mapping of upstream projection cells. The upstream cells directly projecting to the CGRP^{PBN} neurons were retrogradely labeled by using a monosynaptic retrograde tracing based on recombinant rabies virus. Cre-dependent AAV-hsyn-DIO-TVA-HA-N2cG helper virus was unilaterally injected into the PBN of *Calca*^{Cre} mice, followed by SADB19-GFP rabies virus injection two weeks later (**fig. S4A**). Starter cells were detected as double-positive cells for haemagglutinin (HA) and GFP expression, which were found exclusively in the PBN (**fig. S4B**). Consistent with prior tracing studies (*36*), we detected GFP+ retrogradely labeled cells in widely distributed ipsilateral and contralateral brain regions related to

289 emotional processing, sensory, and motor functions, including pIC, CeA, PAG, and
290 superior colliculus (SC) (**fig. S4, C to E)**.

291 We then searched for the projection cells that are activated by looming visual stimuli. To
292 detect activated cells, we used c-Fos as a proxy for neuronal activity. To better isolate
293 looming-specific activation, we included flickering as a control, in which a dark disc
294 simply flickered with no change in size. Separate groups of mice were injected with AAV
295 helper and rabies virus as before but this time bilaterally to label projection cells (**Fig. 3A**
296 **and fig. S5A**). One group was exposed to looming and the other to flickering stimuli,
297 respectively. The looming but not flickering elicited significantly increased freezing
298 compared to the pre-stimuli period (**Fig. 3B**). We focused our c-Fos analysis on the
299 following fear- or vision-related upstream regions: pIC, CeA, PAG, and SC. The
300 percentage of GFP^+ cells that were activated ($c\text{-}Fos^+$) was measured and compared
301 between groups in each brain region. We observed that most of the GFP^+ cells were
302 located in layer 5 and 6 in the pIC and showed a significantly higher percentage of
303 activation in the looming group than the flickering group (**Fig. 3, C and D)**. In the SC, a
304 majority of GFP^+ cells were found in the intermediate layers and they also showed
305 significantly higher percentage of activation in the looming group than in the flickering
306 group (**Fig. 3, C and G)**. However, we found no significant group difference in the CeA
307 and PAG (**Fig. 3, C, E, and F)**. This increased activation in the pIC and SC was specific
308 to the GFP^+ projection cells as there was no group difference in GFP^- cell populations in
309 all brain regions analyzed (**Fig. 3, C to G)**. The results show that the projection cells in
310 the pIC and SC are activated by looming visual stimuli, suggesting the pIC and/or SC may
311 be an upstream region that conveys visual US information to the $CGRP^{PBN}$ neurons.

312

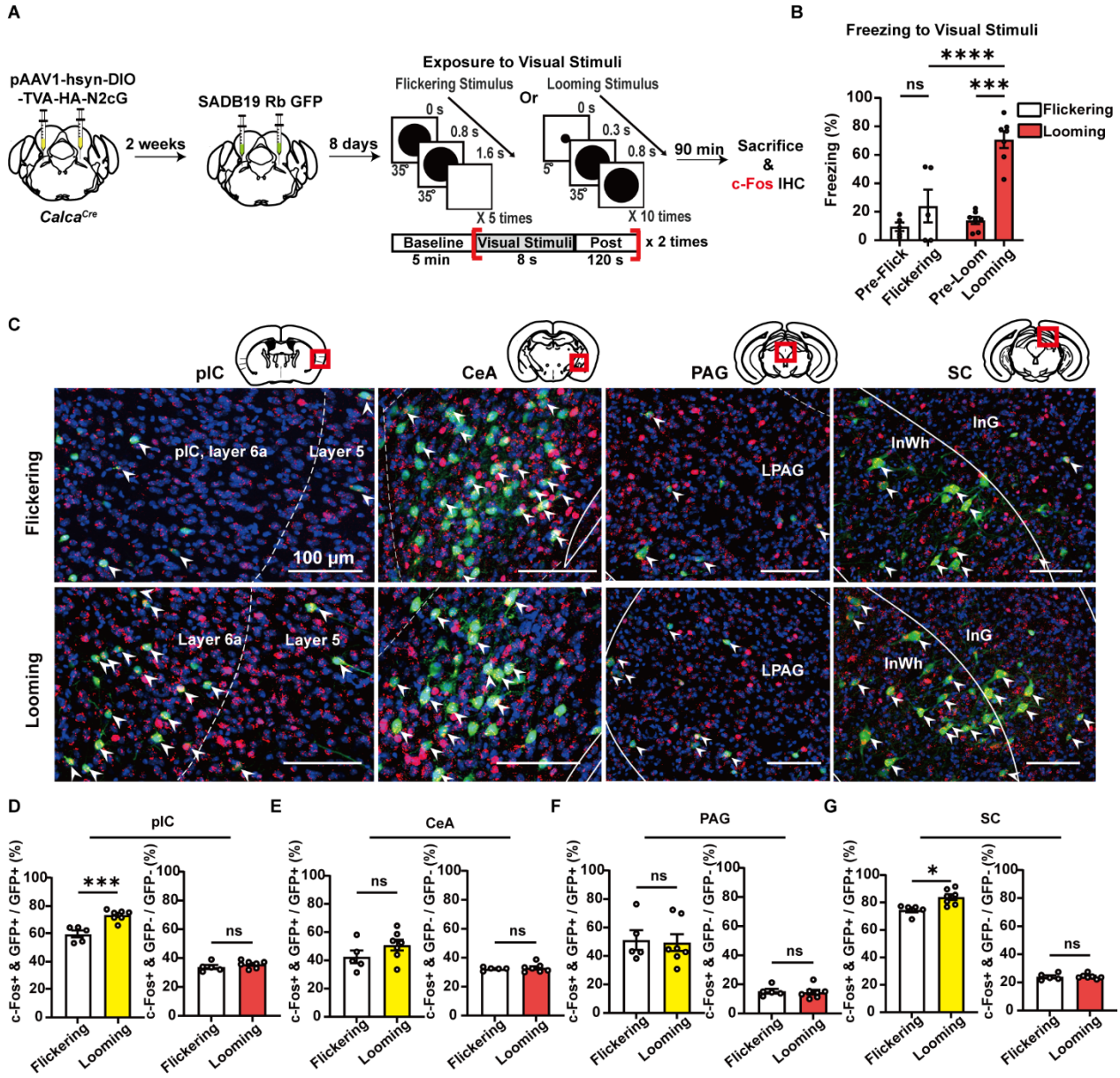

Fig. 3. Identification of CGRP^{PBN}-projecting neurons activated by looming visual stimuli

(**A**) Schematic of a monosynaptic retrograde tracing of CGRP^{PBN} neurons and c-Fos imaging in response to looming stimuli. Bilateral injections of AAV2/1-hsyn-DIO-TVA-HA-N2cG into the PBN of *Calca*^{Cre} mice were followed by bilateral injections of SADB19-GFP rabies virus into the same site. (**B**) Looming visual stimuli induced a robust freezing response in mice, whereas flickering stimuli did not (Flickering, N= 5, Looming, N= 8; RM two-way ANOVA, Time × Group, $F_{1,10}$= 9.893, P< 0.0104). (**C**) Representative confocal microscopic images showing CGRP^{PBN}-projecting GFP+ neurons (Green) and c-Fos+ neurons (Red) in the pIC, CeA, PAG, and SC. A white arrowhead indicates co-localized neurons. Images of starter cells in the PBN are presented in the fig. S5. Scale bars, 100 µm. LPAG, lateral periaqueductal gray; InWh, intermediate white layer of the superior colliculus; InG, intermediate gray layer of the superior colliculus. (**D-G**) The ratio of double-positive neurons (GFP+ & c-Fos+) within GFP+ or GFP- cell populations was compared between the groups (Flickering vs Looming) in each analyzed region: pIC (D) [Flickering, N= 5; Looming, N= 8; Two-tailed unpaired t-test, (left) t_{10}= 4.952, P= 0.0006; (right) t_{10}= 1.145, P= 0.2787], CeA (E) [(left) t_{10}= 1.404, P = 0.1906; (right) t_{10}= 0.4580, P= 0.6567], PAG (F) [(left) t_{10}= 0.2072, P = 0.8400; (right) t_{10}= 0.2809, P= 0.7845], and

SC (G) [(left) t_{10}= 2.593, P= 0.0268; (right) t_{10}= 0.1301, P= 0.8901]. All data are mean ± s.e.m. *p < 0.05. ***p < 0.001. ****p < 0.0001. ns, not significant.

pIC-to-PBN circuit pathway is required for the threat conditioning by looming visual but not by foot-shock stimuli

Previous works in rodents and humans have shown that the insular cortex (IC) is a major hub for processing the cognitive and affective aspects of negative emotions like anxiety, fear, and disgust (*11, 43, 44*). It is thought to play a key role in forming aversive affective states by integrating noxious inputs from both external and internal sources (*45, 65*). Given that the IC responds to both nociceptive stimuli and psychological distress (*46, 47*), and lesions of the IC cause pain asymbolia (*50*), the IC is thought to be more involved in processing affective pain rather than sensory pain. Based on these findings, we focused on the pIC for further studies. We hypothesized that the pIC may transmit threat-relevant aversive affective information to the PBN including $CGRP^{PBN}$ neurons for threat conditioning. As the first step to test this idea, we examined whether the pIC inputs to the PBN are necessary for threat conditioning with the looming US. In order to block this pathway, AAV virus encoding eNpHR3.0 fused with EYFP (or EGFP alone as a control) was injected into the bilateral pIC region, and optic ferrules were implanted in the bilateral PBN (**Fig. 4, A and B**). The axon terminals of pIC neurons in the PBN were inhibited by light during threat conditioning. We found that this optic inhibition did not affect the immediate freezing response to looming stimuli as seen in the case of inhibition of the $CGRP^{PBN}$ neurons (**Fig. 4C**). Importantly, however, this optic inhibition disrupted fear memory formation. During the tone retrieval test, while the control group showed significantly increased freezing to the tone CS, the eNpHR3.0 group showed no significant increase in freezing compared to the pre-CS period (**Fig. 4D**).

We next examined whether this disruption effect is specific. This time, we again optically inhibited the pIC-to-PBN pathway during threat conditioning, but with a foot-shock as a US instead of the looming stimuli. For the foot-shock conditioning, the 20-s tone CS was presented and the last 2-s was paired with a 0.5 mA foot-shock (**Fig. 4, E and F**). This tone-shock pairing was repeated five times with optic inhibition of the pIC-to-PBN terminals during conditioning. The optic inhibition did not affect the defensive escape behavior elicited by the foot-shock (**Fig. 4G**). However, in contrast to the threat conditioning by looming stimuli, the inhibition of the pIC inputs to the PBN had no effect on the threat conditioning by the foot-shock. Mice in both the eNpHR3.0 and control EGFP groups displayed significantly increased freezing to the tone CS compared to the pre-CS period during the tone retrieval test (**Fig. 4H**). Taken together, these results indicate that the pIC neurons provide essential inputs to the PBN for threat conditioning by looming visuals, but this pathway is dispensable for foot-shock threat conditioning.

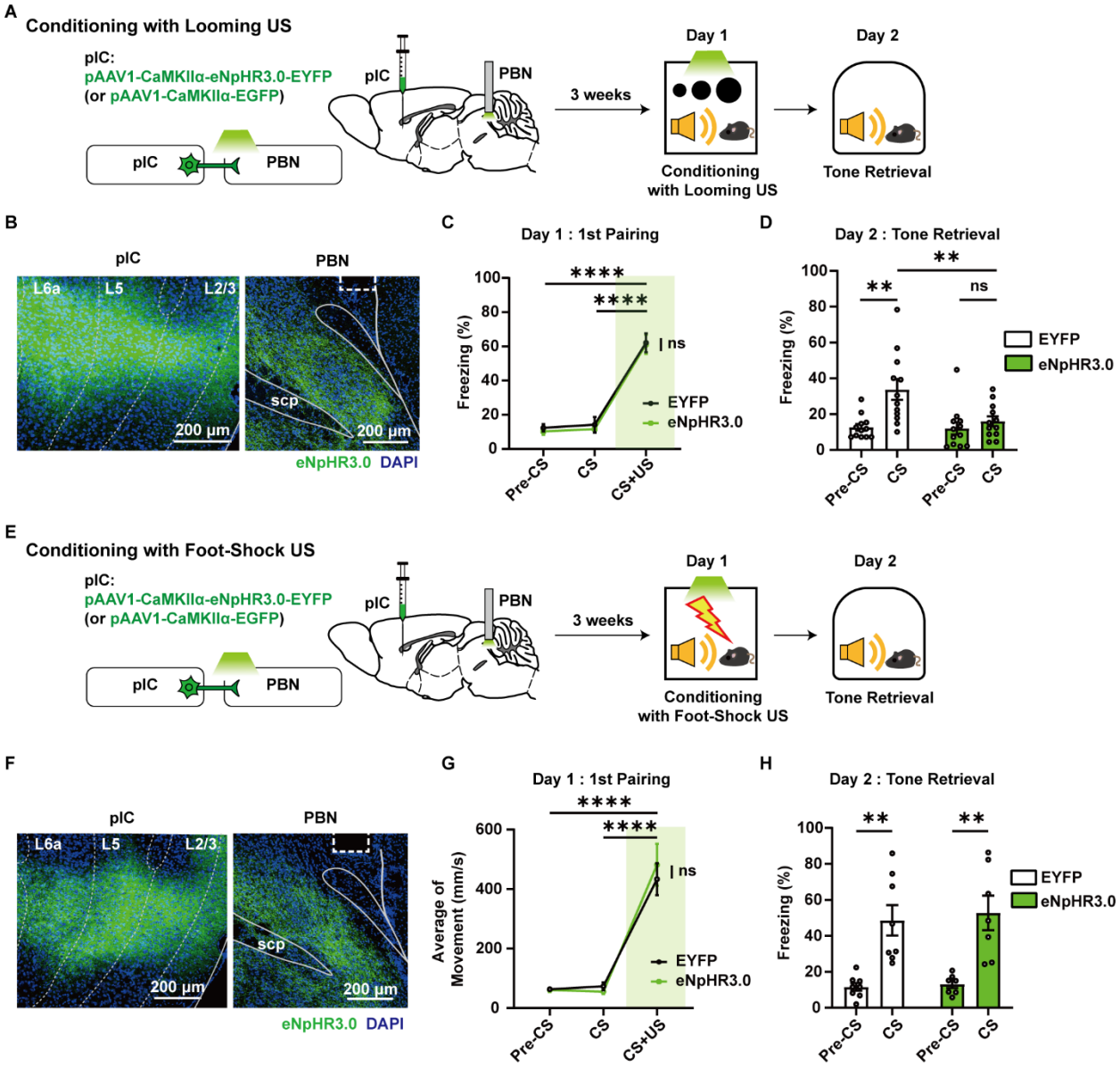

Fig. 4. pIC projections to the PBN is required for threat conditioning with looming but not with foot-shock stimuli

(**A**) Schematic of optogenetic inhibition of pIC-PBN circuit during threat conditioning with looming US. (**B**) Representative images of coronal sections showing the expression of eNpHR3.0-EYFP in the pIC neurons (left) and their axon fibers in the PBN (right). The dotted rectangle in the right panel indicates the location of optic fiber tip. Scale bars, 200 μm. (**C**) Freezing levels during the first pairing of tone CS and looming US on Day 1 (EYFP, N= 12; eNpHR3.0, N =12; RM two-way ANOVA, Time, $F_{2,44}$= 125.6, P< 0.0001). (**D**) Optic inhibition of pIC axon terminals in the PBN during conditioning impaired formation of auditory fear memory (RM two-way ANOVA, Time × Group, $F_{1,22}$= 4.550, P= 0.0443). (**E**) Schematic of optogenetic inhibition of pIC-PBN circuit during foot-shock conditioning. (**F**) Representative confocal microscopic images of coronal sections showing the expression of eNpHR3.0 in the pIC neurons (left) and their axon fibers in the PBN (right). The dotted rectangle in the right panel indicates the location of optic fiber tip. Scale bars, 200 μm. (**G**) Average of movement during the first pairing of tone CS and foot-shock US on Day 1 (EYFP, N = 8; eNpHR3.0, N =7; RM two-way ANOVA, Time, $F_{2,26}$= 71.34, P< 0.0001). (**H**) Optic inhibition of pIC axon terminals in the

385 PBN during foot-shock conditioning did not affect the formation of fear memory (RM two-way
386 ANOVA, Time × Group, $F_{1,13}$= 0.03716, P= 0.8501). All data are mean ± s.e.m. **p < 0.01.
387 ****p < 0.0001. ns, not significant.

388

389 **pIC$^{\rightarrow PBN}$ neurons are required for activation of CGRP^{PBN} neurons in response to**
390 **looming visual but not to foot-shock stimuli.**

391 If pIC is a major upstream region that transmits visual US information to the CGRP^{PBN}
392 neurons, the pIC input should be required for the activation of the CGRP^{PBN} neurons in
393 response to looming stimuli. To test this, we monitored the response of the CGRP^{PBN}
394 neurons to the looming stimuli while selectively inactivating the pIC neurons projecting to
395 the PBN (pIC$^{\rightarrow PBN}$) by using a Designer Receptors Exclusively Activated by Designer
396 Drugs (DREADDs) method. Fiber photometry recordings were conducted to monitor the
397 activity of the CGRP^{PBN} neurons. Because the pIC input to the PBN was not necessary for
398 the shock-driven threat conditioning (**Fig. 4, E to H**), we also tested an effect on the
399 response of the CGRP^{PBN} neurons to the shock in the same mice. For the fiber photometry
400 recordings, Cre-dependent AAV- hsyn-DIO-GCaMP6m virus was injected unilaterally
401 into the PBN of *Calca^{Cre}* mice, and optic ferrule was implanted right above the viral
402 injection sites (**Fig. 5A)**. To selectively express an inhibitory DREADD hM4Di in
403 pIC$^{\rightarrow PBN}$ neurons in the same mice, retrograde AAV virus encoding Flp recombinase
404 (AAVretro-Ef1a-flpO) was injected into the bilateral PBN and Flp-dependent AAV virus
405 encoding hM4Di-mCherry (or mCherry alone as a control) was injected into the bilateral
406 pIC, respectively (**Fig. 5A)**. Post hoc histological analysis confirmed the highly restricted
407 expression of hM4Di-mCherry in the pIC and GCaMP6m in the PBN, respectively (**Fig.**
408 **5B**). Compound 21 (C21), a DREADD agonist (*66*), was administrated to inactivate the
409 pIC$^{\rightarrow PBN}$ neurons 1 hour prior to the photometry recordings. During the photometry
410 recordings, mice were first exposed to the looming stimuli and we observed that calcium
411 response increased in the mCherry group, indicating the activation of CGRP^{PBN} neurons to
412 the looming stimuli (**Fig. 5, C and D**). This increase, however, was absent in the hM4Di
413 group, and we rather observed a gradual decrease in the calcium response (**Fig. 5, C, E,**
414 **and F).** Although unclear, it could mean that an inhibitory GABAergic input is also
415 activated by looming stimuli through a pIC-independent pathway. In contrast to the
416 looming, when exposed to the shock (0.5 mA, 2 s), the hM4Di group showed an increase
417 in the calcium response of the CGRP^{PBN} neurons comparable to the control group (**Fig. 5,**
418 **G to J**). These results indicate that although the CGRP^{PBN} neurons are activated by both
419 looming and shock stimuli, the major input source of activation is different: that is, the
420 pIC input to the PBN is essential for the CGRP^{PBN} neurons' activation to the looming
421 visual but not to the foot-shock stimuli. The same is true for the threat conditioning as
422 shown above (**Fig. 4**).

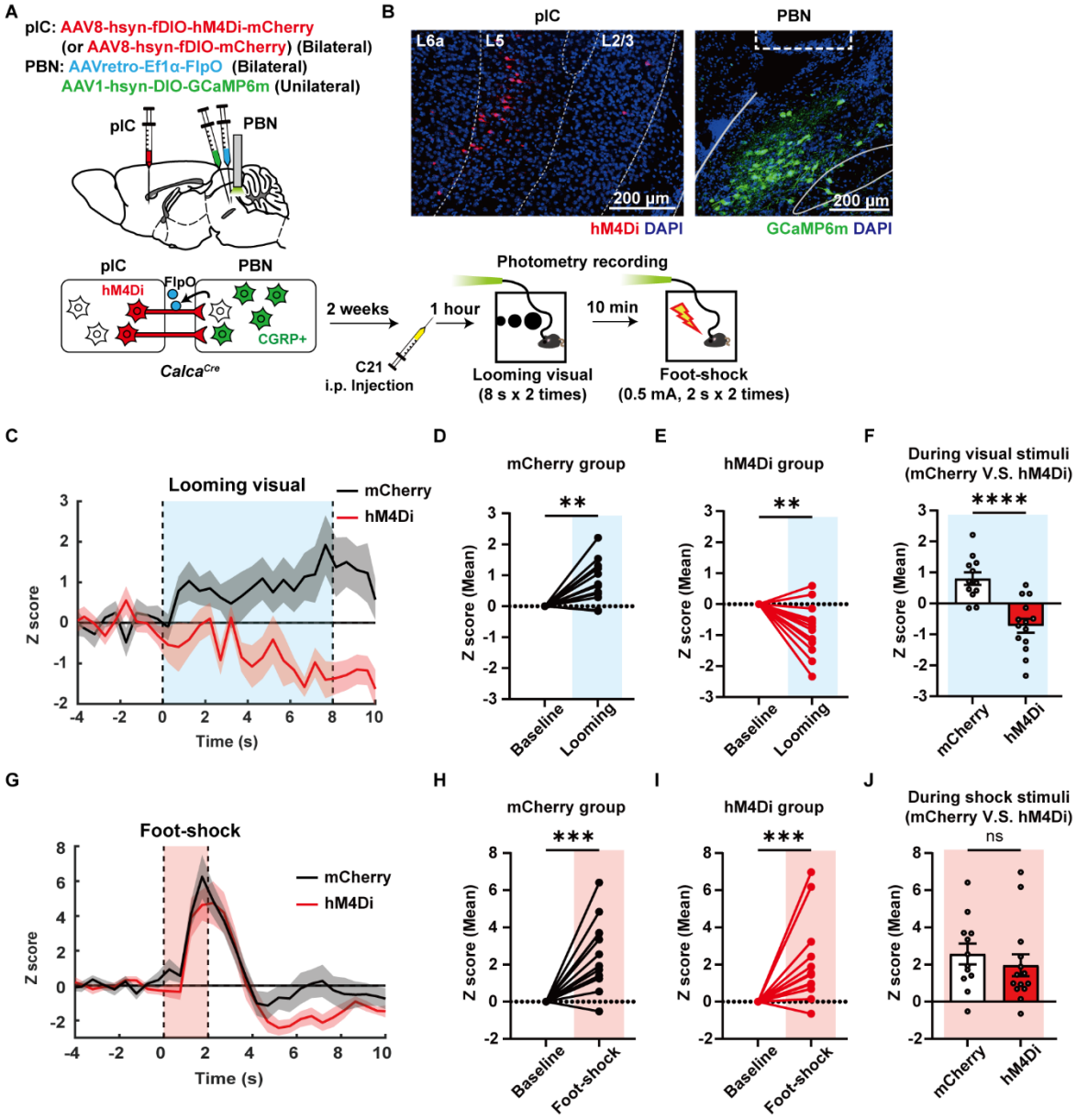

Fig. 5. pIC$^{\rightarrow PBN}$ neurons are necessary for activation of CGRP^{PBN} neurons to looming but not foot-shock stimuli

(**A**) Schematic of photometry recording of CGRP^{PBN} neurons with hM4Di inhibition of pIC$^{\rightarrow PBN}$ neurons. (**B**) Representative images showing expression of hM4Di-mCherry in the pIC$^{\rightarrow PBN}$ neurons (left) and GCaMP6m in CGRP^{PBN} neurons (right). The dotted rectangle indicates the location of optic fiber. Scale bar, 200 μm. (**C**) Z-scored calcium activities of CGRP^{PBN} neurons to visual stimuli. Blue shaded area indicates the visual stimuli window (8 s). (**D-E**) Average calcium activity during visual stimuli in the mCherry group (D) (baseline = −5 to 0 s, looming = 0 to 8 s; N=12 trials; one sample t-test, t_{11}= 3.957, P= 0.0022) and hM4Di group (E) (N =14 trials; t_{13}= 3.216, P= 0.0068). (**F**) Comparison of average changes in calcium activity evoked by looming stimuli between two groups (mCherry, N =12 trials; hM4Di, N =14 trials; two-tailed unpaired t-test, t_{24}= 4.965, P< 0.0001). (**G**) Z-scored calcium activities of CGRP^{PBN} neurons to foot-shock stimuli. Red shaded area indicates the foot-shock window (2 s). (**H-I**) Average calcium activity during foot-shock in the mCherry group (H) (baseline= −5 to 0 s, shock= 0 to 2 s; N =12 trials; one sample t-test, t_{11}= 4.619, P= 0.0007) and hM4Di group (I) (N =14; one sample Wilcoxon test, W= 101.0, P= 0.0004). (**J**) Comparison of average changes in calcium activity evoked by foot-

shock stimuli between two groups (mCherry, N = 12 trials; hM4Di, N =14 trials; two-tailed Mann Whitney test, U= 60, P= 0.2312). All data are mean ± s.e.m. **p < 0.01. ***p < 0.001. ****p < 0.0001. ns, not significant.

One possible interpretation of these calcium activity recording results is that pIC neurons may be selectively responding to the looming visual stimuli. To clarify this point, we targeted the pIC neurons that directly project to the $CGRP^{PBN}$ neurons ($pIC^{\rightarrow CGRP\text{-}PBN}$ neurons) for photometry recordings. To specifically express the calcium indicator GCaMP6s in the target neurons, Cre-dependent AAV-hsyn-DIO-TVA-HA-N2cG helper virus was injected into the unilateral PBN of *Calca*^{Cre} mice. Two weeks later, rabies virus encoding Flp recombinase fused with mCherry was injected into the same injection site and Flp-dependent AAV-Ef1α-fDIO-GCaMP6s virus was injected unilaterally into the pIC, respectively (**fig. S6, A to C**). Photometry recordings revealed that both the looming visual and foot-shock stimuli activate the $pIC^{\rightarrow CGRP\text{-}PBN}$ neurons but with different activation kinetics: a slow increase to the looming stimuli but a rapid increase to the shock (**fig. S6, D to K**). So, it is not that the shock does not activate the pIC neurons but that there is another source, probably a nociceptive input from the spinal cord, that provides a major input to the $CGRP^{PBN}$ neurons in response to the shock. These photometry results also confirm the conclusion derived from the c-Fos analyses that the $pIC^{\rightarrow CGRP\text{-}PBN}$ neurons are activated by looming visual stimuli (**Fig. 3D**).

$pIC^{\rightarrow CGRP\text{-}PBN}$ projections to the PBN induce aversive behavioral states and drive threat conditioning as a US

So far, our data show that pIC-to-PBN circuit is a US pathway for threat conditioning by looming visual stimuli. We hypothesized that this US pathway transmits aversive affective information. To further demonstrate our hypothesis, we investigated whether direct activation of this circuit induces aversive affective states and is sufficient to drive threat conditioning. For these purposes, we targeted the $pIC^{\rightarrow CGRP\text{-}PBN}$ neurons with channelrhodopsin-2 (ChR2) expression and optically stimulated their axon terminals in the PBN (**Fig. 6A**). Cre-dependent AAV helper virus was injected into the bilateral PBN of *Calca*^{Cre} mice and Flp-dependent AAV virus encoding ChR2 fused with EYFP (or EYFP alone) was injected into the bilateral pIC, respectively. Two weeks later, rabies virus encoding Flp recombinase fused with mCherry was injected into the PBN, the same viral injection sites as the helper virus. Post hoc histological analysis confirmed a highly specific expression of ChR2 in the pIC neurons, where Flp-mCherry was also expressed (**Fig. 6B)**. Starter cells were exclusively detected in the PBN (**fig. S5B**). To determine aversive behaviors, we performed a real-time place avoidance (RTPA), open-field test (OFT), and elevated plus maze (EPM) behavior test. In the RTPA test, mice were placed in a three-chamber arena. Either the left or right side was paired with photostimulation of axon terminals of $pIC^{\rightarrow CGRP\text{-}PBN}$ neurons in the PBN in a counter-balanced way. The EYFP control group showed no significant difference in time spent between the light-paired and non-paired chambers (**Fig. 6, C to F**). In contrast, the ChR2 group showed aversion to the light-paired chamber (**Fig. 6, C to F**). In the OFT, a light on and off period was alternated with a 60-s interval (**Fig. 6, G and H**). Compared to the EYFP control, the ChR2 group showed no significant difference in freezing, indicating the photostimulation of the $pIC^{\rightarrow CGRP\text{-}PBN}$ projections in the PBN does not induce freezing (**Fig. 6, H and I**). However, the mice in the ChR2 group showed increased anxiety. They spent less time in the center zone and crossed it fewer times compared to the control mice with similar total

distance traveled between groups (**Fig. 6, J to L**). Lastly, in the EPM test, light stimulation was alternated (2-s on, 2-s off) during the test. The ChR2 group spent less time in the open arms and more time in the closed arms compared to the EYFP control with a significantly fewer open arm entries (**Fig. 6, N to P**). The number of closed arm entries and total movement distance did not differ between groups (**Fig. 6, Q and R**). These results indicate that activation of the pIC→CGRP-PBN projections in the PBN induces aversive affective behavioral states.

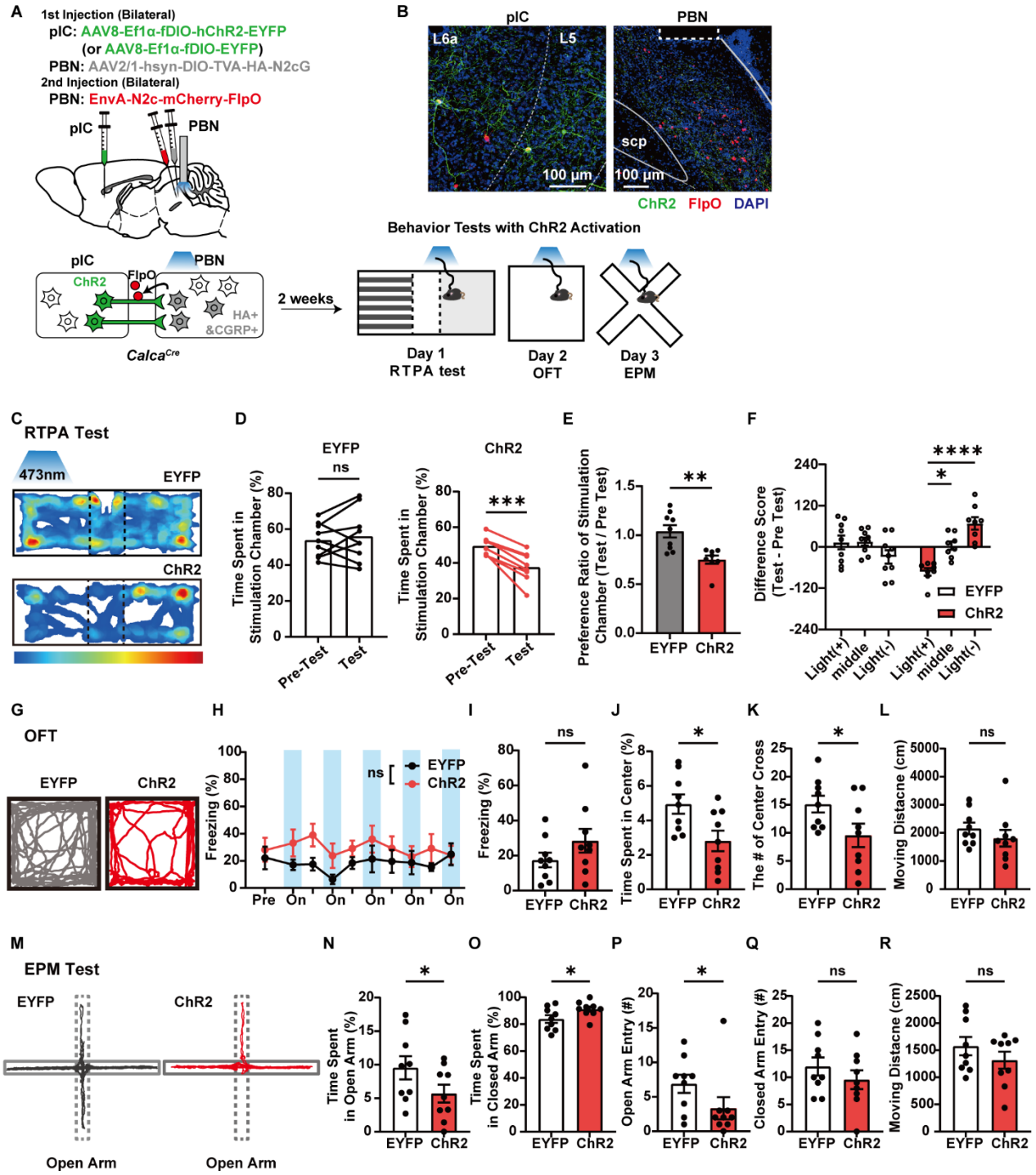

Fig. 6. Optogenetic stimulation of pIC→CGRP-PBN projections in the PBN induces anxiogenic behaviors

(**A**) Schematic of viral injections and behavior tests. (**B**) Representative images of ChR2 (green) and/or retrograde labeled FlpO (Red) expression in the pIC (left) and the PBN (right). The dotted rectangle indicates the location of optic fiber (**C**) Representative heatmaps showing time spent in RTPA test chambers during the photostimulation phase. (**D-F**) ChR2 group showed aversion to the photostimulation-paired chamber in the RTPA test. (D) Time spent in the photostimulated chamber (Left, EYFP; N=9; Two-tailed paired t-test, t_8= 0.6490, P= 0.5345; Right, ChR2; N= 8, t_7= 6.837, P= 0.0002). (E) Preference ratio for the photostimulated chamber (Two-tailed Mann Whitney test, U= 6, P= 0.0025). (F) Difference score for each chamber (RM two-way ANOVA, Time × Group, $F_{2,30}$= 10.77, P= 0.0003). (**G**) Representative movement trajectory during the OFT. (**H-L**) ChR2 group showed increased basal anxiety levels with photostimulation. (H) The photostimulation did not induce a freezing (EYFP, N= 9; ChR2, N= 9; RM two-way ANOVA, Time × Group, $F_{9,144}$= 0.8810, P= 0.5439). Averages of freezing levels (I) (Two-tailed unpaired t-test, t_{16}= 1.379, P= 0.1870), time spent in the center zone (J) (t_{16}= 2.627, P= 0.0183), number of center zone crossings (K) (t_{16}= 2.167, P= 0.0456), and moving distance (L) (t_{16}= 1.131, P= 0.2748). (**M**) Representative movement trajectory during EPM. (**N-R**) Time spent in the open arms (N) (EYFP, N= 9; ChR2, N= 9; t_{16}= 1.765, P= 0.0483), time spent in the closed arms (O) (t_{16}= 2.141, P= 0.0240), number of open arm entries (P) (U= 18.5, P= 0.0495), number of closed arm entries (Q) (t_{16}= 1.012, P=0.1633), and moving distance (R) (t_{16}= 1.129, P= 0.2757) during the EPM test. One-tailed Mann Whitney test in (P) and one-tailed unpaired t-test in (N, O, Q, R) were used. All data are mean ± s.e.m. *p < 0.05. **p < 0.01. ***p < 0.001. ****p < 0.0001. ns, not significant.

We next assessed whether photostimulation of the pIC$^{\rightarrow CGRP\text{-}PBN}$ projections in the PBN can drive threat conditioning as a US. The same viral strategy as above was used to specifically express ChR2 in the pIC$^{\rightarrow CGRP\text{-}PBN}$ neurons (**Fig. 7, A, B, and fig. S5C**). During conditioning, photostimulation of the pIC$^{\rightarrow CGRP\text{-}PBN}$ projections in the PBN was paired with the tone CS five times. During the tone retrieval test, the mice in the ChR2 group, but not in the EYFP control group, exhibited increased freezing to the tone compared to the pre-CS period (**Fig. 7C)**. Overall, these results demonstrate that pIC$^{\rightarrow CGRP\text{-}PBN}$ neurons transmit aversive affective information to the PBN and this pathway is sufficient to drive threat conditioning, identifying a novel threat conditioning circuit.

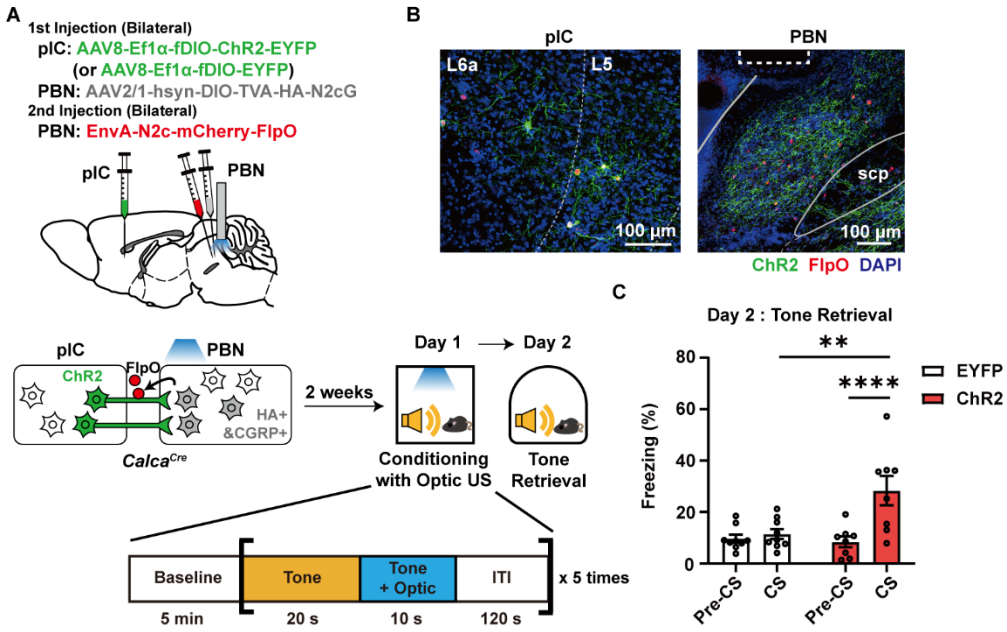

532

533 **Fig. 7. Optogenetic stimulation of pIC$^{\rightarrow CGRP\text{-}PBN}$ projections in the PBN is sufficient to drive**
534 **formation of fear memory**

535 (**A**) Schematic of a threat conditioning paradigm with optogenetic stimulation of pIC$^{\rightarrow CGRP\text{-}PBN}$
536 projections in the PBN as s a US. During conditioning, mice were exposed to a 30-s tone, during
537 which the last 10-s tone presentation was overlapped with optic stimulation. This CS-US pairing
538 was repeated 5 times at a 120-s interval. (**B**) Representative images showing the neurons
539 expressing ChR2 (green) and/or retrograde labeled FlpO (Red) in the pIC (left) and ChR2-
540 expressing neurons projections (green) in the PBN (right). Neurons expressing FlpO were also
541 detected in the PBN (right). The dotted rectangle indicates the location of the optic fiber. Scale
542 bar, 100 μm. (**C**) ChR2-expressing mice exhibited increased freezing levels to the conditioned
543 tone during the fear memory retrieval test (EYFP, N= 9; ChR2, N= 8; RM two-way ANOVA,
544 Time × Group, $F_{1,15}$= 15.22, P= 0.0014). All data are mean ± s.e.m. **p < 0.01. ****p < 0.0001.
545 ns, not significant.
546
547
548

Discussion

In this study, we established a threat conditioning by using looming visual stimuli as a US in mice. Using this model, we identified the projections from pIC$^{\rightarrow CGRP\text{-}PBN}$ neurons to the PBN as a distinct US pathway for threat conditioning. CGRP^{PBN} neurons were required for forming a fear memory and its retrieval. pIC$^{\rightarrow CGRP\text{-}PBN}$ neurons were activated by looming as well as foot-shock stimuli. Stimulation of their projections in the PBN elicited aversive affective states, suggesting that pIC$^{\rightarrow CGRP\text{-}PBN}$ neurons transmit affective information to the PBN. Given the monosynaptic connectivity between pIC$^{\rightarrow CGRP\text{-}PBN}$ and CGRP^{PBN} neurons, it is highly likely that the pIC$^{\rightarrow CGRP\text{-}PBN}$ to CGRP^{PBN} neuronal circuit is a core circuitry for processing visual US information. Intriguingly, whereas essential for visually-driven threat conditioning, the pIC-to-PBN circuit was dispensable for foot-shock conditioning. Thus, the pIC$^{\rightarrow CGRP\text{-}PBN}$ neurons to the PBN pathway seems to serve as a major US pathway for not all but a specific type of sensory stimuli, likely non-nociceptive danger signals.

Importantly, our study isolated separate circuit elements responsible for innate behavioral response and fear learning by a visual threat. Previously, it has been shown that the CGRP neurons (CGRP^{SPFp}) in the thalamic parvocellular subparafascicular nucleus (SPFp), but not the CGRP^{PBN} neurons, are necessary for innate freezing response to looming visual stimuli (*36*). Further advancing this finding, we found not only that inhibition of CGRP^{PBN} neurons by using TetTox and eNpHR3.0 saved innate freezing to looming stimuli as reported previously but also that the same inhibition disrupted fear memory formation. Similarly, optogenetic inhibition of pIC projections to the PBN had no effect on visually-triggered innate freezing response but disrupted fear memory formation. Given CGRP^{PBN} neurons are required for innate freezing to other threats with different sensory modalities (*36*) it seems that the functional dissociation is specific to visual threat. We speculate that it is probably because the looming mimicking a fast-approaching object should elicit rapid and almost reflex-like reactions but fear learning requires a relatively slow risk assessment process mediated by PBN, depending on which the learning may or may not occur. Besides SPFp, other brain regions have been implicated in visually-triggered innate defensive responses. The parabigeminal nucleus (PBGN) receiving projections from parvalbumin positive (PV^{+}) SC neurons (*67*) induces escaping and freezing responses when stimulated. The lateral posterior thalamic nucleus (LPTN) has also been identified as mediating innate responses to looming visual stimuli (*62, 68*). Future studies should investigate to what extent the two pathways (pathway for visually-triggered innate freezing and pathway for threat conditioning) are separated, particularly, from where in the neural circuits the two pathways begin to be diverged.

In this study, two different approaches (c-Fos imaging and fiber photometry) demonstrated that looming stimuli activate the pIC$^{\rightarrow CGRP\text{-}PBN}$ neurons. However, how threat-relevant visual information is relayed to these neurons is unclear. It has been shown that looming stimuli are relayed from retinal ganglion cells to the SC, which then projects to areas such as the PBGN, LPTN, PAG, and VTA, some of which convey this information to the amygdala complex (*62, 67–70*). Considering there are no known direct projections, it is unlikely that pIC$^{\rightarrow CGRP\text{-}PBN}$ neurons were directly activated by inputs from either the retina or SC. Given the reciprocal connectivity between pIC and the amygdala or PBN, these regions could be an input source. Another possibility is that an interoceptive input resulting from physiological changes induced by visual threats may be the potential input driving pIC activation. Interestingly, optogenetic stimulation of PV^{+} SC neurons, a major SC neuronal subtype detecting looming stimuli, increases the heart rate (*67*). In addition, modest activation of CGRP^{PBN} neurons results in moderate tachycardia (*71*).

Optogenetically evoked increase in heart rate enhances anxiety-like behaviors and pIC has been identified as a potential mediator of the bottom-up cardiac interoceptive processing (*72*). Based on these literatures, a cardiac interoceptive pathway could be a potential input source for looming-evoked activation of $pIC^{\rightarrow CGRP\text{-}PBN}$ neurons.

The PBN has long been considered an affective pathway of nociceptive pain. PBN extensively connects to the hypothalamus and CeA (*51,52*), which modulate emotional behaviors and autonomic responses. Specifically, the $CGRP^{PBN}$ neurons to CeA circuit has been shown to be necessary and sufficient for fear learning by a shock (*31*). Previous studies revealed that $CGRP^{PBN}$ neurons have responsiveness to non-nociceptive aversive stimuli as well as nociceptive stimuli (*36*). Besides, it has also been shown that the same population of neurons is inhibited during feeding and activated when satiated (*35*). Based on these findings, it has been proposed that $CGRP^{PBN}$ neurons play a role in comprehensive threat assessment by integrating various external and internal stimuli rather than merely controlling pain-induced behaviors (*73*). Our finding that $CGRP^{PBN}$ neurons are also essential for threat learning by a non-nociceptive visual threat supports this view. Not just fear learning, it has also been shown that the $CGRP^{PBN}$ neurons are sufficient and necessary for conditioned taste aversion (*74*). The current study extends the role of $CGRP^{PBN}$ neurons as a general hub for processing US information for associative learning.

Photometry recordings in this study found that the $CGRP^{PBN}$ neuronal response to the tone CS becomes increased after conditioning. This is in line with a previous report on shock threat conditioning showing increased $CGRP^{PBN}$ activity in response to the conditioned stimulus during the memory retrieval test [Campos et al., 2018 (*35*), but see Kang et al., 2022 (*36*)]. This change in responsiveness of $CGRP^{PBN}$ neurons to the conditioned stimulus could be a cellular mechanism for encoding the acquired danger signal of the conditioned stimulus as a result of conditioning. Consistent with this idea, we found that inactivation of $CGRP^{PBN}$ neurons during the memory retrieval test impaired learned freezing response.

In this study, we tested only one type of non-nociceptive threats, looming visual stimuli, and so, it is unclear to what extent the pIC to PBN circuit we identified as a distinct US pathway for visual threat is generalized to other multi-modal threats. This circuit pathway could be a general US pathway for non-nociceptive threats or specific to only visual threats. It is also possible that somatosensory threats such as an electric foot-shock may be the only exception. Future works using diverse threats encompassing non-nociceptive and nociceptive threats would address this important question. The downstream regions of pIC to PBN circuit mediating threat learning or aversive affective states were not determined in the current study. $CGRP^{PBN}$ neurons are known to project collaterally to several downstream regions with both overlapped and separate contributions to physiological, autonomic, affective changes, and associative fear learning (*71*). It would be interesting to know whether the shared or segregated downstream regions are responsible for looming- and shock-triggered fear learning. Finally, future studies should also test whether pIC to PBN circuit is activated by threats and contributes to fear memory formation in humans and whether this circuit is altered in neuropsychiatric disorders.

In conclusion, our findings provide insights into a top-down circuit mechanism of how a simple pattern of visual stimulus, without accompanying nociception, can induce aversive behavioral states and drive fear memory formation in mice. The discovery of this distinct fear memory circuit broadens our understanding of how threats in environments drive formation of fear memory and helps treat threat-related neuropsychiatric disorders such as PTSD.

Materials and Methods

Mouse strains

Adult (8-24 weeks) C57BL/6J and heterozygous *Calca*^{Cre} (C57BL/6J) mice were used for experiments. Heterozygous *Calca*^{Cre} mice were generated by crossing homozygote *Calca*^{Cre} mice (JAX #033168) and C57BL/6J wild-type mice. Both male and female mice were used in balance, as we did not observe any noticeable differences in behaviors between male and female. Mice were group housed (3-5 mice per cage) under a 12 h light/dark cycle at a constant humidity (40-60%) and temperature (20-24°C). Food and water were available *ad libitum*. All procedures and protocols were approved by the KAIST Institutional Animal Care and Use Committee (KAIST IACUC). All experiments were performed in accordance with the guideline of the KAIST Institutional Animal Care and Use Committee (KAIST IACUC).

Viruses

AAV1-hSyn-DIO-TeTox-P2A-nls-dTomato (5×10^{12} vg/ml), AAV1-hSyn-DIO-tdTomato (8×10^{11} vg/ml), AAV1-Ef1α-DIO-eNpHR3.0-EYFP (1×10^{12} vg/ml), AAV1-CaMKIIα-eNpHR3.0-EYFP (2.5×10^{12} vg/ml), AAV1-CaMKIIα-EGFP (2×10^{12} vg/ml), AAV8-hSyn-fDIO-mCehrry (8×10^{11} vg/ml), AAV8-Ef1α-fDIO-hChR2-EYFP (5×10^{13} vg/ml), AAV8-Ef1α-fDIO-EYFP (3×10^{13} vg/ml) were packaged.

AAV1-Ef1α-DIO EYFP (2×10^{13} vg/ml), AAV8-hSyn-fDIO-hM4Di-mCehrry (2.5×10^{13} vg/ml), AAVretro-Ef1α-FlpO (2.3×10^{13} vg/ml), AAV1-hsyn-DIO-GCaMP6m (1.9×10^{13} vg/ml), AAV8-Ef1α-fDIO-GCaMP6s (1.3×10^{13} vg/ml), AAV1-Ef1α-DIO-FlpO (2.1×10^{13} vg/ml) were purchased from Addgene. AAVdj-hsyn-fDIO-mGFP-2A-Synaptophysin-mRuby was purchased from Stanford gene vector and virus core (GVVC).

The helper and rabies viruses were obtained from the Viral Vector Core facility of the Kavli Institute for Systems Neuroscience, NTNU. The titers of each virus are as follows: AAV-hsyn-DIO-TVA-HA-N2cG (5×10^{11} vg/ml), EnvA pseudotyped SADB19 Rb GFP (1×10^{11} vg/ml), EnvA pseudotyped N2c Rb-mCherry-FlpO (4.4×10^{8} vg/ml). The helper virus was diluted to 5×10^{10} vg/ml in sterile DPBS (Gibco, ThermoFisher) before use for a specific Cre-dependent TVA expression as recommended by a previous paper (*75*).

Virus packaging

Adeno-associated virus (AAV) was packaged as previously described (*76*). The AAV DNA vector constructs used in this study were either obtained by subcloning of plasmids or purchased from addgene. Briefly, we amplified and purified DNA plasmid by using Maxiprep kit (QIAGEN). The prepared DNA vector was co-transfected with the viral vector (pAd ΔF6 and AAV2/1 or AAV2/8) into HEK293T cells (ATCC, #CRL-3216) by using calcium phosphate precipitation. Seventy-two hours after transfection, cells were harvested, and virus was purified on iodixanol gradient by ultracentrifugation. Viral titers were measured by qPCR (Rotor-Gene Q, QIAGEN).

Stereotaxic surgeries

Mice were anesthetized with intraperitoneal injection of pentobarbital (83 mg/kg of body weight). Ophthalmic ointment (Liposic gel, BAUSCH and LOMB) was applied to the

693 eyes of the mice to prevent dehydration. Virus was injected with glass capillary filled with
694 water and 2μl of mineral oil (SIGMA, M5904-500ML) at the tip. The injection pipette was
695 placed at the injection site for additional 10 min post-surgery for diffusion of virus.

696 For manipulation of $CGRP^{PBN}$ neurons, *Calca*^{Cre} mice receives bilateral injection of virus
697 (0.45μl per side) using the following coordinate: PBN (AP -5.0mm, ML ±1.4mm, DV -
698 3.55mm). For optogenetic inhibition of $CGRP^{PBN}$ neurons, the optic fibers (Doric lenses,
699 200μm core diameter, 0.37 NA for optogenetic manipulation) were implanted using the
700 following coordinate: PBN (AP -5.0mm, ML ±1.75mm, DV -3.1mm). For fiber
701 photometry of $CGRP^{PBN}$ neurons, the optic fiber (RWD, 400μm core diameter, 0.5 NA)
702 was implanted unilaterally on the right PBN. The mice underwent behavioral testing after
703 a 2-week recovery period.

704 For unilateral retrograde tracing, *Calca*^{Cre} mice received unilateral injection of helper
705 virus (AAV-hsyn-DIO-TVA-HA-N2cG, 0.45μl) in the right hemisphere of PBN (AP -
706 5.0mm, ML +1.4mm, DV -3.55mm). Two weeks later, rabies virus (EnvA pseudotyped
707 SADB19 Rb GFP, 0.45μl) was injected into the same coordinate. Eight days later, mice
708 were sacrificed for histological analysis. For bilateral retrograde tracing and c-Fos
709 quantification, the injection surgeries were conducted on the bilateral PBN as above. Eight
710 days later, behavioral tests were performed, and mice were sacrificed for histological
711 analysis.

712 To inhibit terminals of pIC-PBN or SC-PBN pathways, C57BL/6J mice received bilateral
713 injection of virus using the following coordinates: pIC (AP -0.4mm, ML ±4.2mm, DV -
714 4.0mm, 0.4μl per side) or SC (AP -3.7mm, ML ±1.2mm, DV -2.0mm, 0.8μl per side). For
715 optogenetic terminal inhibition, optic fiber (Doric Lenses, 200μm core diameter, 0.37NA)
716 was implanted right above the PBN (AP -5.0mm, ML ±1.75mm, DV -3.1mm). Behavioral
717 experiments were conducted 3 weeks after virus injection.

718 For fiber photometry of $CGRP^{PBN}$ neurons with hM4Di inhibition of $pIC^{\rightarrow PBN}$ neurons, we
719 bilaterally injected AAV8-hsyn-fDIO-hM4Di-mCehrry in the pIC and AAVretro-Ef1α-
720 FlpO in the PBN of *Calca*^{Cre} mice. Ten days later, AAV1-hsyn-DIO-GCaMP6m was
721 unilaterally injected into the right PBN (AP -5.0mm, ML +1.4mm, DV -3.55mm), and
722 optic fiber (RWD, 400μm core diameter, 0.5 NA) was implanted on the PBN (AP -5.0mm,
723 ML +1.75mm, DV -3.1mm). After 2-week recovery period, the fiber photometry
724 experiments were conducted.

725 For fiber photometry of $pIC^{\rightarrow CGRP\text{-}PBN}$ neurons, helper virus (AAV-hS-DIO-TVA-HA-
726 N2cG, 0.45μl) was injected into the PBN (AP -5.0mm, ML +1.4mm, DV -3.55mm). Two
727 weeks later, the rabies virus (EnvA pseudotyped N2c Rb-mCherry-FlpO, 0.45μl) was
728 injected into the same site of PBN, and the AAV8-Ef1α-fDIO-GCaMP6s was injected into
729 the ipsilateral pIC (AP -0.4mm, ML +4.2mm, DV -4.0mm, 0.4μl), respectively. Optic
730 fiber (RWD, 400μm core diameter, 0.5 NA) was implanted on the pIC (AP -0.4mm, ML
731 +4.2mm, DV -3.6mm). After a 2-week recovery period, the fiber photometry experiments
732 were conducted.

733 For ChR2 activation of pIC-$CGRP^{PBN}$ circuit, helper virus (AAV-hS-DIO-TVA-HA-
734 N2cG, 0.45μl) was injected into the bilateral PBN (AP -5.0mm, ML ±1.4mm, DV -
735 3.55mm, 0.45μl), and AAV8-Ef1α-fDIO-hChR2-EYFP was injected into the bilateral pIC
736 (AP -0.4mm, ML ±4.2mm, DV -3.6mm, 0.4μl). Two weeks later, the rabies virus (EnvA
737 pseudotyped N2c Rb-mCherry-FlpO, 0.45μl) was injected into the same site of bilateral
738 PBN, and optic fibers (Doric Lenses, 200μm core diameter, 0.37NA) were implanted on
739 the PBN (AP -5.0mm, ML ±1.75mm, DV -3.1mm). After a 2-week recovery period, the
740 ChR2 activation experiments were conducted.

Behavioral procedures

Looming visual stimuli and behavioral apparatus

The looming visual stimuli were generated using custom software in the LabVIEW (National Instruments) environment and displayed on an overhead LCD monitor (38 cm × 22 cm, 60Hz refresh rate, Intehill). The monitor was positioned 30 cm above the mice and presented a white background. For the looming visual stimuli, a dark disc expanded from 5° (2.6 cm) to 35° (18.9 cm) of visual angle over 300 ms, remained on the screen for 500 ms, and was repeated five times (4 s) during conditioning and ten times (8 s) during the behavioral response test, respectively. For the flickering visual stimuli, a 35° (18.9 cm) dark disc appeared on the monitor for 0.8 s, disappeared for 0.8 s, and this sequence was repeated five times (8 s).

The behavioral arena was surrounded by white acrylic walls, with one of the four walls being transparent (35 cm long, 35 cm wide, 30 cm high). During the experiments, the mouse's behavior was recorded through the transparent wall using a video camera positioned diagonally over the arena. The video was captured at a frame rate of 30 FPS using LabVIEW software.

Innate behavioral responses to looming visual stimuli

All animals were handled for 3 days prior to behavioral tests. To assess innate defensive responses to looming visual stimuli, mice were moved to the behavioral arena from their home cages. After more than 2 min of baseline exploration period, mice were exposed to looming visual stimuli for 8 s (10 repetitions of an expanding dark disc). One minute after the exposure to the looming stimuli, animals were removed from the arena and returned to their home cages. To evaluate the habituation effect to the looming visual stimuli, the immediate response test was conducted for 5 consecutive days. In a single-day habituation test, mice were exposed to the visual stimuli ten times, with a 2-min interval between stimuli. The baseline freezing level was measured for 120 s during the pre-stimulus period before the onset of looming visual stimuli, and the looming-evoked freezing level was measured for 8 s during the visual stimuli presentation period.

Open-field test

In the TetTox inhibition experiment, an open field test was performed prior to visual threat conditioning to confirm that there were no differences in basal locomotion and anxiety levels between groups. Mice were placed in an open field arena (45 cm long, 45 cm wide, 30 cm high) and allowed to freely explore for 15 min. Freezing levels, total distance traveled, and time spent in the center area of the arena were measured.

Visual threat conditioning and fear memory retrieval test

All animals were handled for 3 days prior to behavioral tests. The conditioning chamber was a white acrylic box with one transparent wall, measuring 35 cm in length, 35 cm in width, and 30 cm in height. The floor was covered with paper pads. After 5 min of baseline exploration, mice were exposed to a 20-s auditory tone (CS, 2.7 kHz, 80 dB) that was co-terminated with 4-s looming visual stimuli (US, a dark disc expanding five times). After five CS-US pairings with a 2-min interval, mice were removed from the

conditioning chamber. In the unpaired conditioning protocol, the same auditory tone was presented but with random intervals, ranging from 15 to 30 s after the looming visual stimuli. The baseline freezing level was measured for 120 s during the pre-CS period immediately before the tone onset. Freezing levels for the CS and CS+US periods were measured during the first 16 s and last 4 s of CS-US pairing, respectively.

One day after conditioning, an auditory fear memory test was conducted. The mice were placed in a test chamber with a shifted context: a semicircular arena, striped walls, and a white acrylic floor (35 cm long, 35 cm wide, 30 cm high). After more than 2 min of exploration, the conditioned tone was presented for 20 s. Freezing behavior was measured during the pre-CS period (120 s) and the CS period (20 s).

Contextual fear memory test was conducted the following day. Mice were re-exposed to the conditioning chamber for 5 min, and freezing behavior was measured during the first 2 min to assess contextual fear memory.

Foot-shock threat conditioning and fear memory retrieval test

All mice underwent 3 days of handling prior to behavioral testing. For foot-shock conditioning, mice explored a conditioning chamber equipped with a metal grid floor (Med Associates, 25 cm long, 30 cm wide, 20 cm high) for 5 min. Subsequently, they were exposed to a 20-s auditory tone (CS, 2.7 kHz, 80 dB) that was co-terminated with a 2-s foot-shock stimulus (US, 0.5 mA). The CS-US pairing was repeated 5 times with a 2-min interval. The average of baseline movement was measured for 120 s during the pre-CS period immediately before the onset of foot-shock. Movement for the CS and CS+US periods was measured for the first 16 s and the last 4 s during CS-US pairing, respectively.

One day after foot-shock conditioning, an auditory fear memory test was conducted. Mice were placed in a test chamber with a shifted context: a semicircular arena, striped walls, and a white acrylic floor (Med Associates, 25 cm long, 30 cm wide, 20 cm high). After more than 2 min of exploration, the conditioned tone was presented for 20 s. Freezing behavior was measured during the pre-CS period (120 s) and the CS period (20 s).

Optogenetic inhibition behavior experiments

All mice underwent 3 days of handling before behavioral testing and subsequently, these mice were tethered to fiber-optic patch cords for 5 min per day over 3 consecutive days to habituate them to the optic manipulation procedure. For optogenetic eNpHR3.0 inhibition during conditioning, optical inhibition (561nm, continuous, 3-5mW at the fiber tip for soma inhibition, 10mW at the fiber tip for terminal inhibition) was initiated 2 s before the mice were exposed to the first US and was terminated at the end of the experiment. For optogenetic inhibition during the tone retrieval test, optical inhibition was applied during the 20 s when the tone CS was presented and was terminated at the end of the tone CS presentation.

Optogenetic stimulation behavior experiments

All mice underwent 3 days of handling before behavioral testing. Additionally, mice were tethered to fiber-optic patch cords for 5 min per day over 3 consecutive days to habituate them to the optic manipulation procedure.

To assess the anxiogenic effects of stimulating the pIC-CGRP^{PBN} pathway, we conducted the RTPA test, open-field test, and elevated plus maze (EPM) test sequentially. In the RTPA test, the three-chamber arena was used (25 cm long, 75 cm wide, and 25 cm high; two side chambers with 30 cm wide each, and a middle chamber with 15 cm wide). One of the side chambers had a striped wall and metal grid floor, while the other had a checkered wall and punched metal floor. During the test, mice explored the arena for total 30 min. The first 10-min was used to determine a baseline chamber preference between the two side chambers. The chamber with more preference was selected for pairing with photostimulation. During the last 10 min, optical stimulation (473 nm, 20 Hz, 10 ms pulse, 10 mW at the fiber tip) was applied only when mice entered the selected side chamber. To assess the avoidance behavior induced by photostimulation, the time spent in each side chamber during the pre-test (the first 10 min) and test period (the last 10 min) was compared. The preference ratio was calculated by dividing the time spent in the photostimulation-paired chamber during the test by the time spent in the same chamber during the pre-test. The difference score was calculated by subtracting time spent in each chamber (left, middle, and right) during the pre-test from during the test. One mouse that spent more than 70% of the time in one of the two side chambers during the pre-test period was excluded from the analysis.

In the open-field test, to evaluate the effect of optical stimulation on immediate freezing and anxiogenic behaviors, mice were allowed to explore an open-field arena (45 cm x 45 cm x 30 cm). After 2-min exploration, the mice were exposed to a 30 s-photostimulation (473 nm, 20 Hz, 10 ms pulse, 10 mW at the fiber tip) session five times with a 60-s interval. Measures included freezing behavior, time spent in the center zone, the number of center crossings, and total distance traveled. The center zone was defined as a 20 cm square area in the center of the arena.

In the EPM test, the arena was a cross-shaped acrylic structure with 65 cm in length and 5 cm in width. Two closed arms were enclosed by 16 cm high white acrylic walls, while the open arms have 0.5 cm high transparent acrylic walls. Mice were allowed to explore the EPM arena freely for 10 min, during which they were exposed to photostimulation with a 2-s on and 2-s off cycle. To evaluate anxiety behavior, the time spent in the open and closed arms, the number of entries into each arm, and the total distance traveled during the 10-min test were measured.

For optic conditioning, mice were allowed to explore a conditioning chamber equipped with a metal grid floor (Med Associates, 25 cm long, 30 cm wide, 20 cm high) for 5 min. Subsequently, they were exposed to a 30-s auditory tone (CS, 2.7 kHz, 80 dB) that was co-terminated with a 10-s photostimulation (US, 473 nm, 20 Hz, 10 ms pulse, 10 mW at the fiber tip). The CS-US pairing was repeated 5 times with a 2-min interval. One day after conditioning, mice were tested for auditory fear memory. Mice were placed in a test chamber with a shifted context: a semicircular arena, striped walls, and a white acrylic (Med Associates, 25 cm long, 30 cm wide, 20 cm high). After more than 2 min of exploration, the conditioned tone was presented for 30 s. Freezing behavior was measured during the pre-CS period (120 s) and the CS period (30 s).

c-Fos imaging behavior experiments

To assess c-Fos levels in the projection neurons upstream to CGRP^{PBN} neurons in response to looming visual stimuli, behavioral experiments were conducted 8 days after rabies virus injection. Mice were allowed to freely explore the test arena for 5 min before being exposed to visual stimuli (either looming visual stimuli for 8 s with 10 expansions

878 or flickering visual stimuli for 8 s with 5 flickers) twice at a 120-s interval. The mice were
879 then returned to their home cages and sacrificed 90 min after the first stimulus exposure.

880

881 **Fiber photometry**

882 For fiber photometry, a 400 μm diameter, 0.48 NA patch cord was used to collect
883 fluorescence emission. A real-time signal processor [Tucker-Davis Technologies (TDT),
884 RZ5P) controlled the 470 nm (Thor Labs, M470F3) and 405 nm (Doric, LEDC1-405_FC)
885 LEDs and simultaneously recorded GCaMP fluorescence emission. The 470 nm LED was
886 sinusoidally modulated at 331 Hz to excite GCaMP, while the 405 nm LED was
887 modulated at 531 Hz to monitor the isosbestic signal. The 470nm and 405nm light passed
888 through a bandpass filter in a mini cube (Doric, FMC5), and into the optic fiber connected
889 to the brain of mice. The emitted GCaMP6m signal was detected by a photoreceiver (New
890 Focus, Model 2151) and digitized at 1017.3 Hz by the RZ5P processor. Fluorescence
891 measurements (<6 Hz) were extracted from Synapse software (TDT), and further data
892 processing was performed in MATLAB. ΔF/F was calculated by applying a least-squares
893 linear fit to the 405 nm signal, aligning it with the 470 nm signal (fitted 405nm), and then
894 computing ΔF/F as (470 nm - fitted 405 nm)/fitted 405 nm.

895 Behavioral experiments were recorded at 30 FPS, with stimulus delivery and video
896 capture controlled by a custom LabView program. To synchronize photometry recording
897 with behavioral events (e.g., tone, visual stimuli, shock), digital signals generated by
898 LabView were recorded by the RZ5P processor. To compare ΔF/F across animals during
899 stimulus exposure, ΔF/F was normalized to a Z-score, calculated as [(ΔF/F – Mean of
900 $\Delta F/F_{baseline}$)/Std of $\Delta F/F_{baseline}$], where the baseline mean and standard deviation were
901 computed from –5 to 0 s before stimulus onset.

902 To record calcium activity of $CGRP^{PBN}$ neurons while inhibiting $pIC^{\rightarrow PBN}$ neurons chemo-
903 genetically, DREADD agonist 21 dihydrochloride (C21; Tocris, #6422; 0.2 mg/ml
904 working solution, 10 mg/ml stock) was administered via i.p. injection at a dose of 1
905 mg/kg. One hour after the C21 injection, mice were placed in the looming test chamber,
906 where they explored for 5 min before being exposed to the looming visual stimuli
907 comprising 10-consecutive looming stimulus twice at a 120-s interval. After a 10-min rest,
908 mice were moved to a foot-shock chamber, where they explored for 5 min before being
909 exposed to two foot-shocks (2s, 0.5mA) at a 120-s interval.

910 To record the calcium response of $pIC^{\rightarrow CGRP\text{-}PBN}$ neurons to either looming or foot-shock
911 stimuli, mice were first placed in the looming test chamber and allowed to freely explore
912 the chamber for 5 min and then subsequently exposed to looming visual stimuli as above
913 (10 consecutive looming stimulus twice at a 120-s interval). After a 10-min rest, the mice
914 were transferred to the foot-shock chamber, where they were allowed to freely explore the
915 chamber for 5 min and then received a foot-shock (2s, 0.5mA) twice at a 120-s interval.
916 Because $pIC^{\rightarrow CGRP\text{-}PBN}$ neurons showed a sustained increase in calcium activity in
917 response to both the looming and shock stimuli, we included only the recording data
918 obtained from the first 120-s window from the onset of stimuli for the analysis.

919

920 **Analysis of behaviors**

921 Freezing was defined as a state in which the mouse remained completely immobile except
922 for respiratory movements. Running was defined as when the centroid of the mouse body
923 moved at a velocity of 40 cm/s or greater. All other behaviors were classified as no

response. The centroid of the subjects was analyzed to determine position, calculate velocity, and track movement trajectories. Centroid was detected by using custom MATLAB scripts. Brightness thresholds were manually set to differentiate the pixels corresponding to the mouse. Perspective distortion from the camera lens was corrected using the *tform* function in MATLAB. Velocity was calculated from the centroid data and smoothed using a mean filter.

Histology

For histological verification of virus expression and optic fiber placement, brain sections were prepared from the sacrificed mice after the end of behavioral experiments. Mice were anesthetized with 2.5% avertin by intraperitoneal injection, and they were perfused transcardially with phosphate-buffered saline (PBS) and then fixed with ice cold 4% paraformaldehyde (PFA). After perfusion, brain samples were stored in 4% PFA overnight for post-fixation and sliced in a 40μm thickness afterward by using a vibratome (VT-1200S, Leica Microsystems).

For a retrograde tracing and c-Fos staining, mice underwent behavioral experiments 8 days after the rabies virus injection and were sacrificed 90 min after exposure to visual stimuli. Mice were anesthetized with pentobarbital (83 mg/kg of body weight) by intraperitoneal injection, perfused transcardially with phosphate-buffered saline (PBS), and then fixed with ice cold 4% paraformaldehyde (PFA). After perfusion, brain samples were stored in 4% PFA overnight for post-fixation. Fixed brain samples were dehydrated in a series of 10%, 20%, and 30% filtered sucrose solutions (#S0389, Sigma-Aldrich) until they sank to the bottom of vials. Dehydrated brain samples were attached on a specimen disc with OCT compounds (#4583, Scigen) at -20 ℃. Brains were coronally sliced in a 40μm thickness by using a Cryostat (Leica CM1850, Leica Biosystems).

Brain sections were mounted on a gelatin-coated slide glass with a Vectashield antifade mounting media (h-2000, Vector Laboratories). Images were taken for histological verification by using a confocal microscope (LSM880, Carl ZEISS) or slide scanner (ZEISS Axio Scan.Z1, Carl ZEISS). By reference to the Mouse Brain Atlas, the mice who showed off-target viral expression in surrounding areas or displacement of ferrules were excluded.

Immunohistochemistry

For immunostaining, brain sections were washed three times with PBS and incubated in blocking solution (2% goat serum, 0.1% BSA, and 0.2% Triton X-100 in PBS) for 1 hour on an orbital shaker (126 rpm). Brain sections were incubated in a primary antibody solution on the orbital shaker (126 rpm) overnight at room temperature (RT). After brain sections were washed four times with PBS, sections were then incubated in a secondary antibody solution on the shaker (126 rpm) for 2 hours. Subsequently, the brain sections underwent four additional washes with PBS. Immunostained brain sections were transferred to gelatin-coated slides using a brush. Sections were stained with DAPI (0.5μg/ml in PBS; #D9542, Sigma-Aldrich) for 20min at RT. The slides were rapidly immersed in a distilled water and allowed to air-dry completely in a light-protected environment. Coverslip was mounted with a Vectashield antifade mounting media (h-2000, Vector Laboratories).

969 The dTomato fluorescence signals in neurons injected with AAV-TetTox-P2A-nls-
970 dTomato virus were amplified with mouse anti-DsRed primary antibody (1:500; #SC-
971 390909, Santacruz) and Alexa Fluor 594-conjugated goat anti-mouse secondary antibody
972 (1:2000; #A-11005, Molecular Probes). The EYFP fluorescence signals in neurons
973 injected with AAV-CaMKIIα-eNpHR3.0-EYFP virus were amplified with rabbit anti-GFP
974 primary antibody (1:5000; #ab290, abcam) and Alexa Fluor 488-conjugated goat anti-
975 rabbit secondary antibody (1:2000; #A-11008, Molecular Probes). The antibodies used for
976 HA staining were rabbit anti-HA (1:1000; #3724, Cell signaling) and Alexa Fluor 647-
977 conjugated goat anti-rabbit (1:2000; #A-21244, Molecular Probes). The antibodies used
978 for c-Fos staining were rabbit anti-cFos (rabbit anti-cFos; 1:2000; #226008, Synaptic
979 systems) and Alexa Fluor 594-conjugated goat anti-rabbit (Alexa Fluor 594-conjugated
980 goat anti-rabbit; 1:2000; #A-11037, Molecular Probes).

981

982 **Cell counting analysis**

983 To map the location of retrogradely labeled GFP+ cells throughout the whole brain,
984 coronal brain tissues were collected along AP axis (from anterior part AP +1.8 mm to
985 posterior part AP: -5.5 mm) in a 120-µm distance. For the brain-wide tracing, images of
986 all brain sections were captured using a Slide scanner (ZEISS Axio Scan.Z1, Carl ZEISS).
987 The number of DAPI+ and GFP+ cells in the brain sections were then counted by using
988 the AMaSiNe automatic cell counting software (*77*) by registering brain images to the
989 Allen Brain Atlas Common Coordinate Framework (CCFv3) (*78*).

990 To assess the overlap between c-Fos+ and GFP+ cells, we conducted c-Fos
991 immunostaining, and optical sections (2 µm per section) were obtained using confocal
992 microscopy with Z-stack analysis. DAPI+, GFP+, and c-Fos+ cells were detected using
993 the AMaSiNe cell counting algorithm (*77*). Regions of interest (ROI) were then defined in
994 each target area, and the overlap between c-Fos+ and GFP+ cells was manually counted in
995 a blinded manner. The AP ranges for c-Fos quantification in each target brain area are:
996 pIC (AP -0.2 to -0.6 mm), CeA (AP -1.2 to -1.6 mm), PAG (AP -3.5 to -3.9 mm), SC (AP
997 -3.5 to -3.9 mm).

998

999 **Statistical analysis**

1000 GraphPad Prism 10.0.2 was used for graph generation and statistical analyses. The
1001 Shapiro-Wilk test was conducted to assess data normality. Paired or unpaired Student's t-
1002 tests were performed to compare normally distributed datasets of experimental and control
1003 groups depending on experimental design. Wilcoxon matched-pairs signed rank test or
1004 Mann Whitney test were performed to compare non-normally distributed datasets of
1005 experimental and control groups. One-way ANOVA and repeated-measures two-way
1006 ANOVA, followed by Sidak's post-hoc test, were used to analyze behavioral tasks
1007 depending on the experimental design. Differences were considered statistically
1008 significant if the p-value was below 0.05. Error bars represent the s.e.m.
1009
1010

References

1. T. Beckers, D. Hermans, I. Lange, L. Luyten, S. Scheveneels, B. Vervliet, Understanding clinical fear and anxiety through the lens of human fear conditioning. *Nat. Rev. Psychol.* **2**, 233-245 (2023).

2. J. E. LeDoux, Emotion, memory and the brain. *SCI AM* **270**, 50-57 (1994).

3. M. S. Fanselow, What is conditioned fear?. *TINS* **7**, 460-462 (1984).

4. J. E. LeDoux, Emotion circuits in the brain. Annu. Rev. Neurosci. **23**, 155-184 (2000).

5. J. F. Medina, J. Christopher Repa, M. D. Mauk, J. E. LeDoux, Parallels between cerebellum-and amygdala-dependent conditioning. *Nat. Rev. Neurosci.* **3**, 122-131 (2002).

6. J. P. Johansen, C. K. Cain, L. E. Ostroff, J. E. LeDoux, Molecular mechanisms of fear learning and memory. *Cell* **147**, 509-524 (2011).

7. C. T. Gross, N. S. Canteras, The many paths to fear. *Nat. Rev. Neurosci.* **13**, 651-658 (2012).

8. P. Tovote, J. P. Fadok, A. Lüthi, Neuronal circuits for fear and anxiety. *Nat. Rev. Neurosci.* **16**, 317-331 (2015).

9. P. Rainville, B. Carrier, R. K. Hofbauer, M. C. Bushnell, G. H. Duncan, Dissociation of sensory and affective dimensions of pain using hypnotic modulation. *Pain* **82**, 159-171 (1999).

10. M. A. Lumley, J. L. Cohen, G. S. Borszcz, A. Cano, A. M. Radcliffe, L. S. Porter, H. Schubiner, F. J. Keefe, Pain and emotion: a biopsychosocial review of recent research. *J. Clin. Psychol.* **67**, 942-968 (2011).

11. T. Singer, B. Seymour, J. O'doherty, H. Kaube, R. J. Dolan, C. D. Frith, Empathy for pain involves the affective but not sensory components of pain. *Science* **303**, 1157-1162 (2004).

12. D. D. Price, Psychological and neural mechanisms of the affective dimension of pain. *Science* **288**, 1769-1772 (2000).

13. A. C. D. C. Williams, K. D. Craig, Updating the definition of pain. *Pain* **157**, 2420-2423 (2016).

14. K. D. Venkateswaran, C. T. Hauser, Living with PTSD amid a global pandemic. *Psychol. Trauma* **12,** S71 (2020).

15. R. Zimering, S. B. Gulliver, J. Knight, J. Munroe, T. M. Keane, Posttraumatic stress disorder in disaster relief workers following direct and indirect trauma exposure to Ground Zero. *JTS* **19**, 553-557 (2006).

16. A. Pinchevski, Screen trauma: Visual media and post-traumatic stress disorder. *Theory Cult. Soc.* **33**, 51-75 (2016).

17. M. W. Otto, A. Henin, D. R. Hirshfeld-Becker, M. H. Pollack, J. Biederman, J. F. Rosenbaum, Posttraumatic stress disorder symptoms following media exposure to tragic events: Impact of 9/11 on children at risk for anxiety disorders. *J. Anxiety Disord.* **21**, 888-902 (2007).

18. K. J. Wallace, J. B. Rosen, Predator odor as an unconditioned fear stimulus in rats: elicitation of freezing by trimethylthiazoline, a component of fox feces. *Behav. Neurosci.* **114**, 912 (2000).

19. R. J. Blanchard, M. Yang, C. I. Li, A. Gervacio, D. C. Blanchard, Cue and context conditioning of defensive behaviors to cat odor stimuli. *Neurosci Biobehav Rev* **25**, 587-595 (2001).

20. L. K. Takahashi, Olfactory systems and neural circuits that modulate predator odor fear. *Front. behav. neurosci.* **8**, 72 (2014).

21. A. Cruz, M. Heinemans, C. Marquez, M. A. Moita, Freezing displayed by others is a learned cue of danger resulting from co-experiencing own freezing and shock. *Curr. Biol.* **30**, 1128-1135 (2020).

22. S. Maren, Neurobiology of Pavlovian fear conditioning. *Annu. Rev. Neurosci.***24**, 897-931 (2001).

23. H. C. Pape, D. Pare, Plastic synaptic networks of the amygdala for the acquisition, expression, and extinction of conditioned fear. *Physiol. Rev.* **90**, 419-463 (2010).

1055 24. J. E. LeDoux, Coming to terms with fear. *Proc. Natl. Acad. Sci. U.S.A.* **111**, 2871-2878 (2014).

1056 25. B. A. Pellman, J. J. Kim, What can ethobehavioral studies tell us about the brain's fear
1057 system? *TINS* **39**, 420-431 (2016).

1058 26. R. P. Vertes, S. B. Linley, W. B. Hoover, Limbic circuitry of the midline thalamus. *Neurosci*
1059 *Biobehav Rev* **54**, 89-107 (2015).

1060 27. L. G. Reijmers, B. L. Perkins, N. Matsuo, M. Mayford, Localization of a stable neural correlate of
1061 associative memory. *Science* **317**, 1230-1233 (2007).

1062 28. P. W. Frankland, B. Bontempi, L. E. Talton, L. Kaczmarek, A. J. Silva, The involvement of the
1063 anterior cingulate cortex in remote contextual fear memory. *Science* **304**, 881-883 (2004).

1064 29. J. A. Boatman, J. J. Kim, A thalamo-cortico-amygdala pathway mediates auditory fear
1065 conditioning in the intact brain. *EJN* **24**, 894-900 (2006).

1066 30. J. P. Johansen, H. L. Fields, Glutamatergic activation of anterior cingulate cortex produces an
1067 aversive teaching signal. *Nat. Neurosci.* **7**, 398-403 (2004).

1068 31. S. Han, M. T. Soleiman, M. E. Soden, L. S., Zweifel, R. D. Palmiter, Elucidating an affective
1069 pain circuit that creates a threat memory. *Cell* **162**, 363-374 (2015).

1070 32. K. E. Krout, A. S. Jansen, A. D. Loewy, Periaqueductal gray matter projection to the parabrachial
1071 nucleus in rat. *J. Comp. Neurol.* **401**, 437-454 (1998).

1072 33. A. J. Todd, Neuronal circuitry for pain processing in the dorsal horn. *Nat. Rev. Neurosci.* **11**, 823-
1073 836 (2010).

1074 34. S. P. Hunt, P. W. Mantyh, The molecular dynamics of pain control. *Nat. Rev. Neurosci.* **2**, 83-91
1075 (2001).

1076 35. C. A. Campos, A. J. Bowen, C. W. Roman, R. D. Palmiter, Encoding of danger by parabrachial
1077 CGRP neurons. *Nature* **555**, 617-622 (2018).

1078 36. S. J. Kang, S. Liu, M. Ye, D. I. Kim, G. M. Pao, B. A. Copits, B. Z. Roberts, K. F. Lee, M. R.
1079 Bruchas, S. Han, A central alarm system that gates multi-sensory innate threat cues to the
1080 amygdala. *Cell Rep.* **40**, (2022).

1081 37. L. K. Takahashi, M. M. Chan, M. L. Pilar, Predator odor fear conditioning: current perspectives
1082 and new directions. *Neurosci Biobehav Rev* **32**, 1218-1227 (2008).

1083 38. D. C. Blanchard, G. Griebel, R. J. Blanchard, Conditioning and residual emotionality effects of
1084 predator stimuli: some reflections on stress and emotion. *Prog Neuropsychopharmacol Biol Psychiatry*
1085 **27**, 1177-1185 (2003).

1086 39. L. K. Takahashi, D. T. Hubbard, I. Lee, Y. Dar, S. M. Sipes, Predator odor-induced conditioned
1087 fear involves the basolateral and medial amygdala. *Behav. Neurosci.* **121**, 100 (2007).

1088 40. N. S. Pentkowski, D. C. Blanchard, C. Lever, Y. Litvin, R. J. Blanchard, Effects of lesions to the
1089 dorsal and ventral hippocampus on defensive behaviors in rats. *EJN* **23**, 2185-2196 (2006).

1090 41. D. C. Blanchard, N. S. Canteras, C. M. Markham, N. S. Pentkowski, R. J. Blanchard, Lesions of
1091 structures showing FOS expression to cat presentation: effects on responsivity to a Cat, Cat odor, and
1092 nonpredator threat. *Neurosci Biobehav Rev* **29**, 1243-1253 (2005).

1093 42. M. Rodríguez, F. Ceric, P. Murgas, B. Harland, F. Torrealba, M. Contreras, Interoceptive insular
1094 cortex mediates both innate fear and contextual threat conditioning to predator odor. *Front. behav.*
1095 *neurosci.* **13**, 283 (2020).

1096 43. M. P. Paulus, M. B. Stein, An insular view of anxiety. *Biol Psychiatry* **60**, 383-387 (2006).

1097 44. D. A. Gehrlach, N. Dolensek, A. S. Klein, R. R. Chowdhury, A. Matthys, M. Junghänel, T. N.
1098 Gaitanos, A. Podgornik, T. D. Black, N. R. Vaka, K.-K. Conzelmann, N. Gogolla, Aversive state
1099 processing in the posterior insular cortex. *Nat. Neurosci.* **22**, 1424-1437 (2019).

1100 45. A. S. Klein, N. Dolensek, C. Weiand, N. Gogolla, Fear balance is maintained by bodily feedback
1101 to the insular cortex in mice. *Science* **374**, 1010-1015 (2021).

1102 46. H. Gündel, M. F. O'Connor, L. Littrell, C. Fort, R. D. Lane, Functional neuroanatomy of grief: an
1103 FMRI study. *Am J Psychiatry* **160**, 1946-1953 (2003).

1104 47. N. I. Eisenberger, M. D. Lieberman, K. D. Williams, Does rejection hurt? An fMRI study of
1105 social exclusion. *Science* **302**, 290-292 (2003).

1106 48. T. Klucken, S. Kagerer, J. Schweckendiek, K. Tabbert, D. Vaitl, R. Stark, Neural, electrodermal
1107 and behavioral response patterns in contingency aware and unaware subjects during a picture–picture
1108 conditioning paradigm. *Neurosci.* **158**, 721-731 (2009).

1109 49. J. B. Nitschke, I. Sarinopoulos, K. L. Mackiewicz, H. S. Schaefer, R. J. Davidson, Functional
1110 neuroanatomy of aversion and its anticipation. *Neuroimage* **29**, 106-116 (2006).

1111 50. N. Grahek, *Feeling pain and being in pain*. (mit Press, 2011)

1112 51. T. L. Krukoff, K. H. Harris, J. H. Jhamandas, Efferent projections from the parabrachial nucleus
1113 demonstrated with the anterograde tracer Phaseolus vulgaris leucoagglutinin. *BRB* **30**, 163-172 (1993).

1114 52. K. Tokita, T. Inoue, J. D. Boughter Jr., Afferent connections of the parabrachial nucleus in
1115 C57BL/6J mice. *Neuroscience* **161**, 475-488 (2009).

1116 53. D. C. Blanchard, C. Markham, M. Yang, D. Hubbard, E. Madarang, R. J. Blanchard, Failure to
1117 produce conditioning with low-dose trimethylthiazoline or cat feces as unconditioned stimuli. *Behav.*
1118 *Neurosci.* **117**, 360 (2003).

1119 54. M. Yilmaz, M. Meister, Rapid innate defensive responses of mice to looming visual
1120 stimuli. *Curr. Biol.* **23**, 2011-2015 (2013).

1121 55. G. De Franceschi, T. Vivattanasarn, A. B. Saleem, S. G. Solomon, Vision guides selection of
1122 freeze or flight defense strategies in mice. *Curr. Biol.* **26**, 2150-2154 (2016).

1123 56. G. Baranauskas, N. Svirskiene, G. Svirskis, 20 Hz membrane potential oscillations are driven by
1124 synaptic inputs in collision-detecting neurons in the frog optic tectum. *Neurosci. Lett.* **528**, 196-200
1125 (2012).

1126 57. T. W. Dunn, C. Gebhardt, E. A. Naumann, C. Riegler, M. B. Ahrens, F. Engert, F. Del Bene,
1127 Neural circuits underlying visually evoked escapes in larval zebrafish. *Neuron* **89**, 613-628 (2016).

1128 58. K. Bhattacharyya, D. L. McLean, M. A. MacIver, Visual threat assessment and reticulospinal
1129 encoding of calibrated responses in larval zebrafish. *Curr. Biol.* **27**, 2751-2762 (2017).

1130 59. W. Schiff, J. A. Caviness, J. J. Gibson, Persistent fear responses in rhesus monkeys to the optical
1131 stimulus of "looming". *Science* **136**, 982-983 (1962).

1132 60. J. Náñez Sr, Perception of impending collision in 3-to 6-week-old human infants. *Infant Behav.*
1133 *Dev.* **11**, 447-463 (1988).

1134 61. W. Schiff, Perception of impending collision: A study of visually directed avoidant
1135 behavior. *Psychol. Monogr.* **79**, 1 (1965).

1136 62. P. Wei, N. Liu, Z. Zhang, X. Liu, Y. Tang, X. He, B. Wu, Z. Zhou, Y. Liu, J. Li, Y. Zhang, X.
1137 Zhou, L. Xu, L. Chen, G. Bi, X. Hu, F. Xu, L. Wang, Processing of visually evoked innate fear by a
1138 non-canonical thalamic pathway. *Nat. Commun.* **6**, 6756 (2015).

1139 63. J. C. Kim, M. N. Cook, M. R. Carey, C. Shen, W. G. Regehr, S. M. Dymecki, Linking genetically
1140 defined neurons to behavior through a broadly applicable silencing allele. *Neuron* **63**, 305-315 (2009).

1141 64. M. E. Carter, M. E. Soden, L. S. Zweifel, R. D. Palmiter, Genetic identification of a neural circuit
1142 that suppresses appetite. *Nature* **503**, 111-114 (2013).

1143 65. D. Kargl, J. Kaczanowska, S. Ulonska, F. Groessl, L. Piszczek, J. Lazovic, K. Buehler, W.
1144 Haubensak, The amygdala instructs insular feedback for affective learning. *Elife* **9**, e60336 (2020).

66. X. Chen, H. Choo, X. P. Huang, X. Yang, O. Stone, B. L. Roth, J. Jin, The first structure–activity relationship studies for designer receptors exclusively activated by designer drugs. *ACS Chem. Neurosci.* **6**, 476-484 (2015).

67. C. Shang, Z. Liu, Z. Chen, Y. Shi, Q. Wang, S. Liu, D. Li, P. Cao, A parvalbumin-positive excitatory visual pathway to trigger fear responses in mice. *Science* **348**, 1472-1477 (2015).

68. C. Shang, Z. Chen, A. Liu, Y. Li, J. Zhang, B. Qu, F. Yan, Y. Zhang, W. Liu, Z. Liu, X. Guo, D. Li, Y. Wang, P. Cao, Divergent midbrain circuits orchestrate escape and freezing responses to looming stimuli in mice. *Nat. commun.* **9**, 1232 (2018).

69. D. A. Evans, A. V. Stempel, R. Vale, S. Ruehle, Y. Lefler, T. Branco, A synaptic threshold mechanism for computing escape decisions. *Nature* **558**, 590-594 (2018).

70. Z. Zhou, X. Liu, S. Chen, Z. Zhang, Y. Liu, Q. Montardy, Y. Tang, P. Wei, N. Liu, L. Li, R. Song, J. Lai, X. He, C. Chen, G. Bi, G. Feng, F. Xu, L. Wang, VTA GABAergic neural circuit mediates visually evoked innate defensive responses. *Neuron* **103**, 473-488 (2019).

71. A. J. Bowen, J. Y. Chen, Y. W. Huang, N. A. Baertsch, S. Park, R. D. Palmiter, Dissociable control of unconditioned responses and associative fear learning by parabrachial CGRP neurons. *Elife* **9**, e59799 (2020).

72. B. Hsueh, R. Chen, Y. Jo, D. Tang, M. Raffiee, Y. S. Kim, M. Inoue, S. Randles, C. Ramakrishnan, S. Patel, D. K. Kim, T. X. Liu, S. H. Kim, L. Tan, L. Mortazavi, A. Cordero, J. Shi, M. Zhao, T. T. Ho, A. Crow, A.-C. W. Yoo, C. Raja, K. Evans, D. Bernstein, M. Zeineh, M. Goubran, K. Deisseroth, Cardiogenic control of affective behavioural state. *Nature* **615**, 292-299 (2023).

73. R. D. Palmiter, The parabrachial nucleus: CGRP neurons function as a general alarm. *TINS* **41**, 280-293 (2018).

74. J. Y. Chen, C. A. Campos, B. C. Jarvie, R. D. Palmiter, Parabrachial CGRP neurons establish and sustain aversive taste memories. *Neuron* **100**, 891-899 (2018).

75. T. J. Roelofs, S. Menting-Henry, L. M. Gol, A. M. Speel, V. H. Wielenga, K. M. Garner, M. C. M. Luijendijk, A. A. Hennrich, K. K. Conzelmann, R. A. Adan, Optimization of whole-brain rabies virus tracing technology for small cell populations. *Sci. Rep.* **11**, 10400 (2021).

76. J. T. Kwon, R. Nakajima, H. S. Kim, Y. Jeong, G. J. Augustine, J. H. Han, Optogenetic activation of presynaptic inputs in lateral amygdala forms associative fear memory. *Learn. Mem.* **21**, 627-633 (2014).

77. J. H. Song, W. Choi, Y. H. Song, J. H. Kim, D. Jeong, S. H. Lee, S. B. Paik, Precise mapping of single neurons by calibrated 3D reconstruction of brain slices reveals topographic projection in mouse visual cortex. *Cell Rep.* **31**, (2020).

78. Q. Wang, S. L. Ding, Y. Li, J. Royall, D. Feng, P. Lesnar, N. Graddis, M. Naeemi, B. Facer, A. Ho, T. Dolbeare, B. Blanchard, N. Dee, W. Wakeman, K. E. Hirokawa, A. Szafer, S. M. Sunkin, S. W. Oh, A. Bernard, J. W. Phillips, M. Hawrylycz, C. Koch, H. Zeng, J. A. Harris, L. Ng, The Allen mouse brain common coordinate framework: a 3D reference atlas. *Cell* **181**, 936-953 (2020).

Acknowledgments

We thank all members of the Memory Biology laboratory for helpful comments, discussions, and constructive suggestions. We thank the KAIST Bio-Core Center and the KAIST Analysis Center for Research Advancement (KARA) for use of confocal microscopes and assistance in performing imaging experiments.

Funding: This work was supported by grants from the National Research Foundation of Korea (NRF-2022M3E5E8081183 and NRF-2017M3C7A1031322).

Author contributions:

Conceptualization: J.H., J-H.H.
Methodology: J.H., J-H.H.
Investigation: J.H., B.S.
Analysis: J.H., B.S.
Visualization: J.H.
Supervision: J-H.H.
Writing—original draft: J.H.
Writing—review & editing: J.H., B.S., J-H.H.

Competing interests:

Authors declare that they have no competing interests.

Data and materials availability:

All data necessary to understand and assess the conclusions of this manuscript are presented in the paper and the supplemental information. Codes for detecting position of mouse and analyzing calcium activities are available upon request. Any additional information required to reanalyze the data reported in this paper is available from the lead contact upon request.

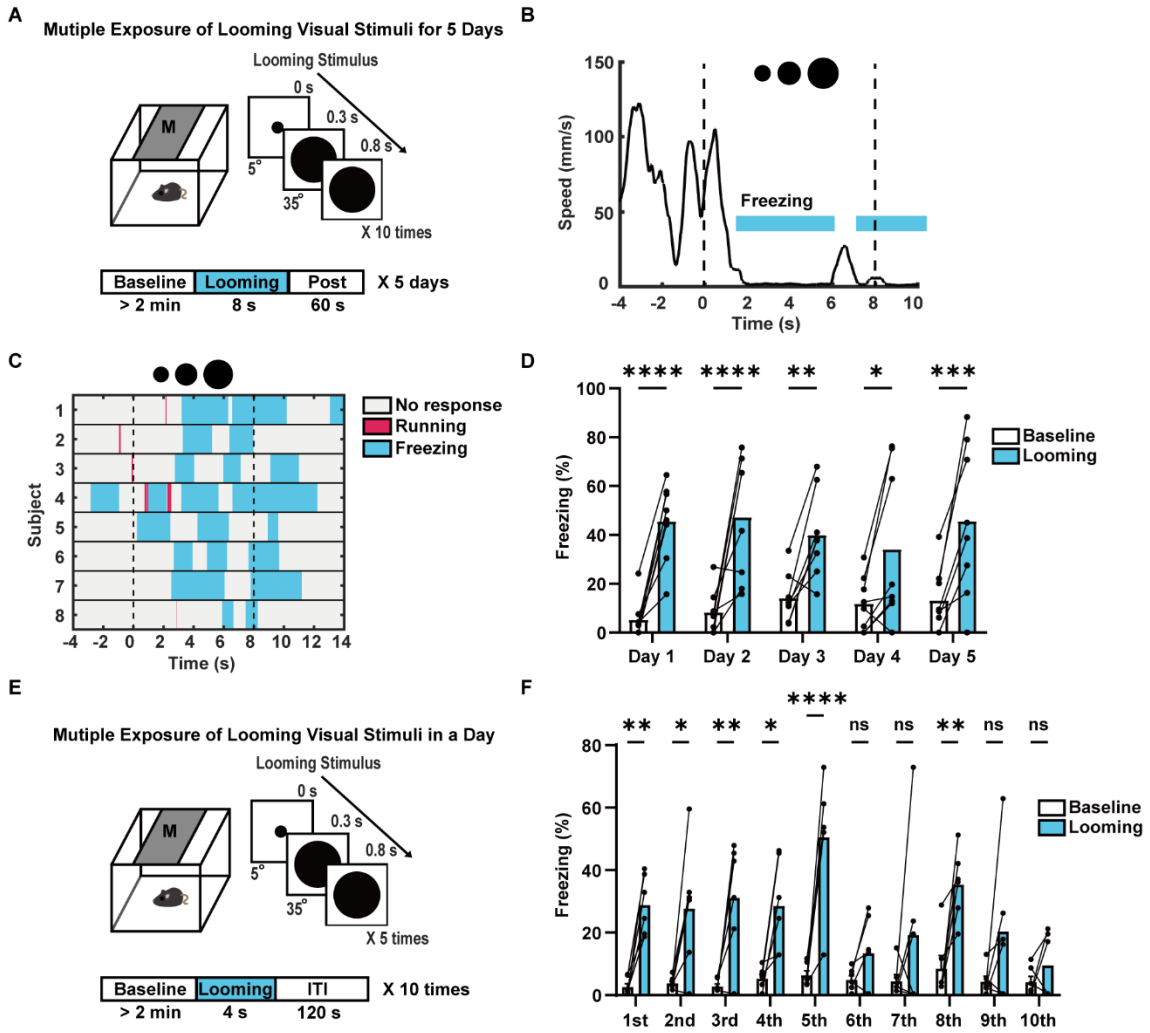

Fig. S1. Innate defensive behavioral responses to looming visual stimuli and habituation. (related to Figure 1).

(**A**) Schematic of repeated behavioral tests for innate defensive responses to looming visual stimuli over 5 days. On each day, mice were exposed to looming visual stimuli (a 10-times repeat of a single looming for 8 s). (**B**) Changes in movement speed of mice in response to looming visual stimuli. The blue shaded bars indicate a period during which mice displayed freezing behavior. (**C**) Ethogram showing defensive behavioral responses to the presentation of looming visual stimuli on day 1. Mice mainly displayed freezing with a rare running response. (**D**) No significant habituation to the daily presented looming stimuli over 5 days. Freezing response to looming visual stimuli was maintained over 5 days (N = 8 mice; RM two-way ANOVA, Stimulus, $F_{1,7}$= 52.27, P= 0.0002). (**E**) Schematic of a behavioral test for innate freezing response to a pattern of looming visual stimuli, which was repeated with a short time interval. A 5-times repeat of a single looming for 4 s was repeated 10 times at a 120-s interval. (**F**) Habituation of innate freezing response. Freezing was measured for each 4-s looming (N = 6 mice; RM two-way ANOVA, Day × Stimulus, $F_{9,90}$= 2.281, P= 0.0236). All data are mean ± s.e.m. *p < 0.05. **p < 0.01. ***p < 0.001. ****p < 0.0001. ns, not significant.

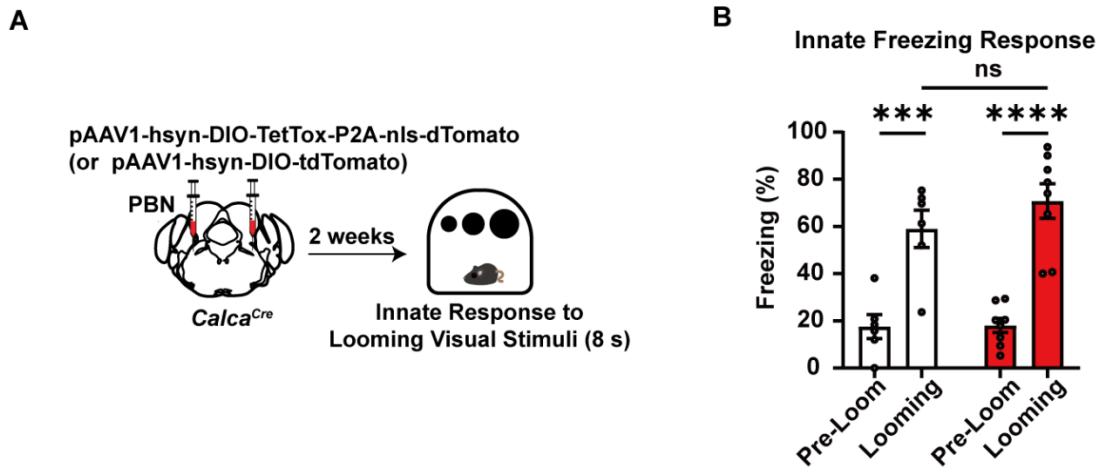

Fig. S2. TetTox inhibition of CGRP^{PBN} neurons did not impair innate defensive behavioral responses to looming visual stimuli (related to Figure 2).

(**A**) Schematic of innate freezing response test with TetTox-mediated inhibition of CGRPPBN neurons. (**B**) TetTox inhibition of the CGRP^{PBN} neurons did not affect innate freezing response to looming visual stimuli (tdTomato group, $N = 6$ mice; TetTox group, $N = 8$ mice; RM two-way ANOVA, Group, $F_{1,12} = 0.8939$, $P = 0.3631$).

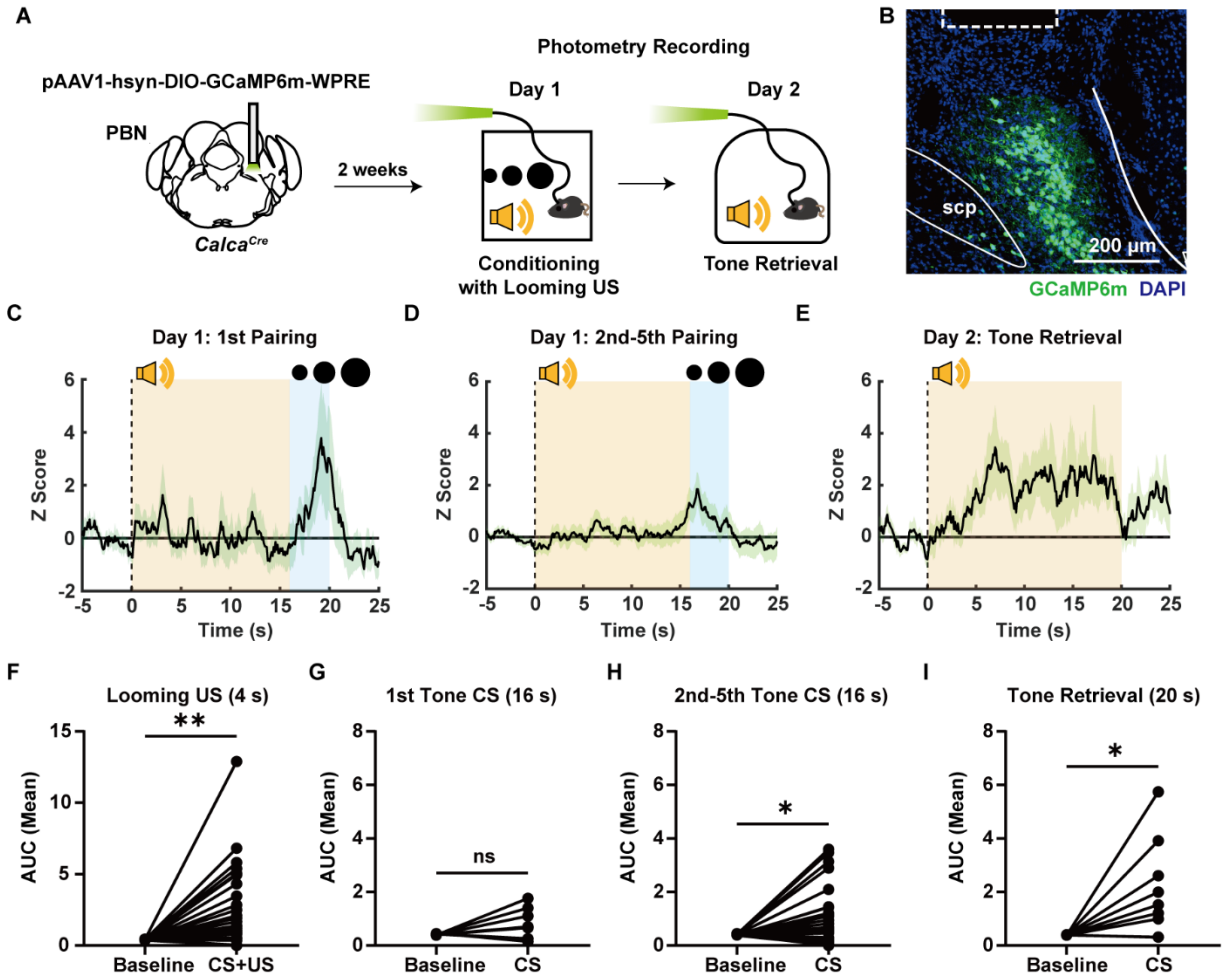

Fig. S3. Response of CGRP^{PBN} neurons to the tone CS becomes increased after threat conditioning with looming US (related to Figure 2).

(**A**) Schematic of fiber photometry recordings of CGRP^{PBN} cell populations during conditioning with looming US. Unilateral injection of AAV1-hsyn-DIO-GCaMP6m and optic fiber implantation into the PBN of *Calca^{Cre}* mice. (**B**) Representative confocal microscopic image of coronal section showing the expression of GCaMP6m in the PBN of *Calca^{Cre}* mice. The dotted rectangle indicates the location of optic fiber. (**C-E**) Z-scored calcium activities (mean ± s.e.m) of CGRP^{PBN} cell populations during the first CS-US pairing (C), during the 2nd-5th CS-US pairings (D), and during the tone retrieval test (E). (**F-I**) Average area under curve (AUC) of calcium activity during 1st-5th exposures to looming visual stimuli [N= 45 trials (5 trials per mouse, 9 mice); two-tailed Wilcoxon matched-pairs signed rank test, W= -561.0, P= 0.0012] (F), during the first exposure of tone CS [N = 9 trials (1 trial per mouse, 9 mice); two-tailed paired t-test, t_8= 1.551, P= 0.1595] (G), during the 2nd-5th presentation of tone CS [N =36 trials (4 trials per mouse, 9 mice); two-tailed Wilcoxon matched-pairs signed rank test, W=-284.0, P= 0.0249] (H), and during the tone retrieval test [N = 9 trials (1 trial per mouse, 9 mice); two-tailed paired t-test, t_8= 2.808, P= 0.0229] (I). All data are mean ± s.e.m. *p < 0.05. **p < 0.01. ns, not significant.

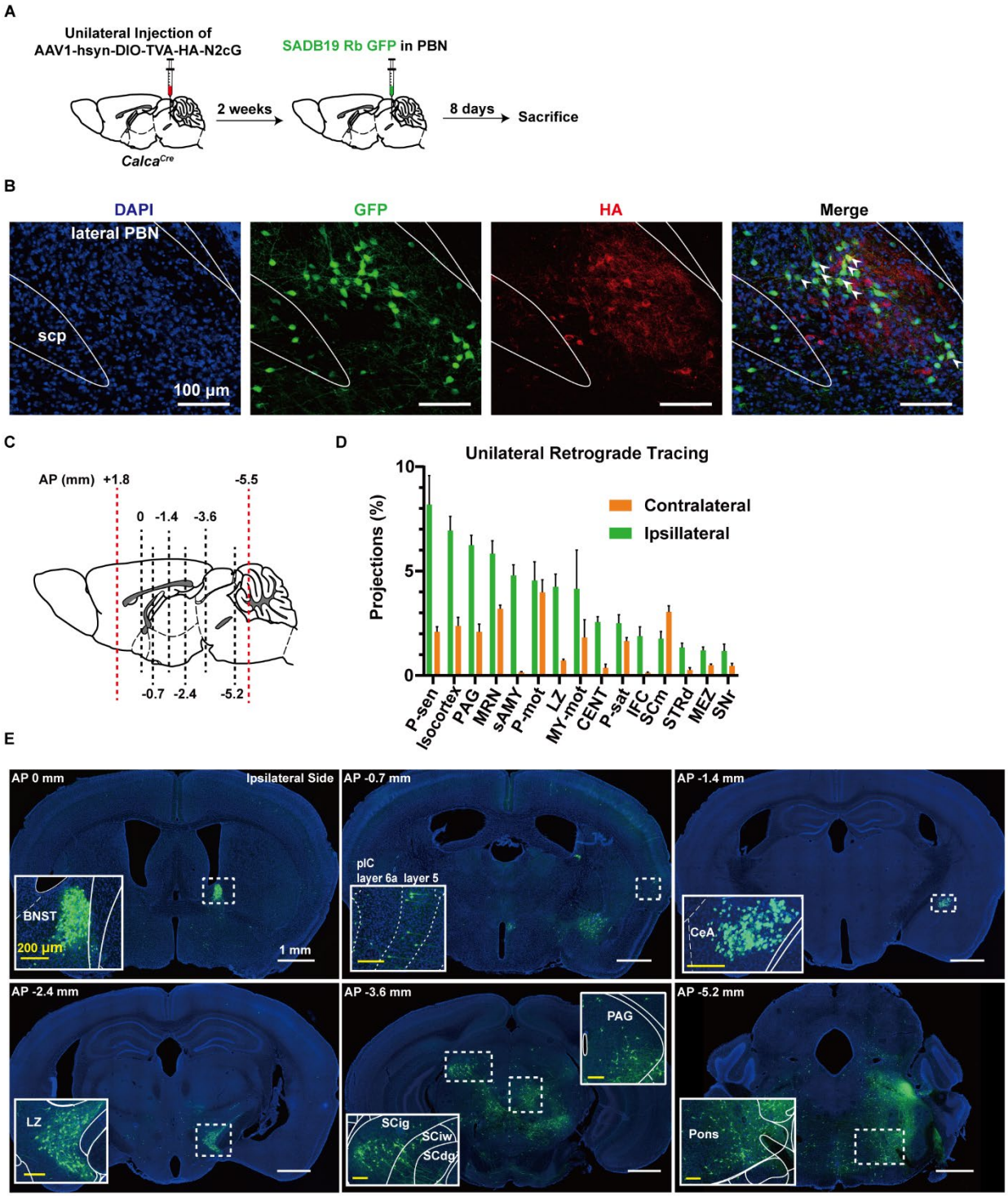
A
Unilateral Injection of
AAV1-hsyn-DIO-TVA-HA-N2cG
SADB19 Rb GFP in PBN
2 weeks
8 days
Sacrifice
Calca^Cre
B
DAPI
GFP
HA
Merge
lateral PBN
scp
100 µm
C
AP (mm) +1.8
-5.5
0 -1.4 -3.6
-0.7 -2.4 -5.2
D
Unilateral Retrograde Tracing
Projections (%)
Contralateral
Ipsillateral
P-sen
Isocortex
PAG
MRN
sAMY
P-mot
LZ
MY-mot
CENT
P-sat
IFC
SCm
STRd
MEZ
SNr
E
AP 0 mm
Ipsilateral Side
BNST
200 µm
1 mm
AP -0.7 mm
plC
layer 6a layer 5
AP -1.4 mm
CeA
AP -2.4 mm
LZ
AP -3.6 mm
PAG
SCig
SCiw
SCdg
AP -5.2 mm
Pons

Fig. S4. Brain-wide monosynaptic retrograde tracing of CGPR^{PBN} neurons (related to Figure 3).

(**A**) Schematic of unilateral monosynaptic retrograde tracing of CGRP^{PBN} neurons. Unilateral injections of AAV2/1-hsyn-DIO-TVA-HA-N2cG into the PBN of *Calca*^{Cre} mice were followed by unilateral injections of SADB19-GFP rabies virus into the same site 2 weeks later. (**B**) Representative confocal microscopic images of coronal sections showing neurons expressing GFP and/or haemagglutinin (HA) tag in the PBN. White arrows indicate double-positive starter cells (GFP+ & HA+). Scale bar, 100 µm. (**C**) The range of AP coordinates where coronal sections were collected for imaging analysis (AP, +1.8 mm to -5.5 mm, indicated by dotted red lines) and the AP coordinates at which representative images shown in panel (E) were taken (dotted black lines). (**D**) Percentage of projections of the top 15 regions with the highest number of retrogradely labeled neurons. (**E**) Representative confocal microscopic images of coronal sections showing the retrogradely labeled neurons with GFP in each target region analyzed. Inset is a magnified view of the dotted box in each corresponding region. Scale bars: 1 mm (white bar) and 200 µm (yellow bar in insets), respectively.

Abbreviations: Pons, sensory related (P-sen); Periaqueductal gray (PAG); Midbrain reticular nucleus (MRN); Striatum-like amygdalar nuclei (sAMY); Pons, motor related (P-mot); Hypothalamic lateral zone (LZ); Medulla, motor related (MY-mot); Central lobule (CENT); Pons, behavioral state related (P-sat); Inferior colliculus (IFC); Superior colliculus, motor related (SCm); Striatum dorsal region (STRd); Hypothalamic medial zone (MEZ); Substantia nigra, reticular part (SNr); Posterior insular cortex (pIC); central amygdalar nucleus (CeA); Superior colliculus, motor related, intermediate gray layer (SCig); Superior colliculus, motor related, intermediate white layer (SCiw); Superior colliculus, motor related, deep gray layer (SCdg).

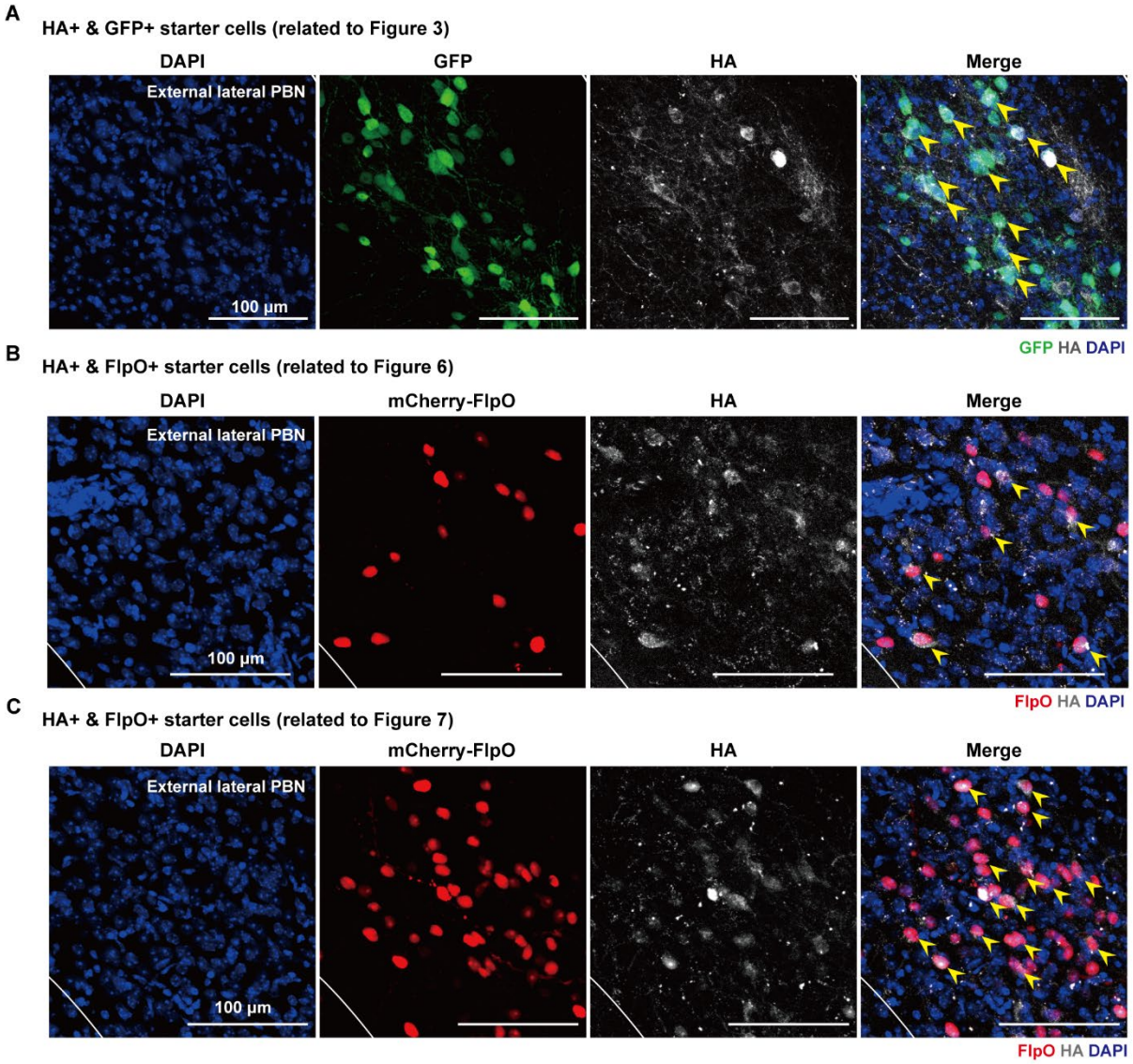

Fig. S5. Images of starter cells in the PBN in the monosynaptic retrograde labelling experiments (related to Figure 3, 6, and 7).

(**A**) Representative confocal microscopic images of coronal sections showing the neurons double positive for GFP and HA tag in the PBN. Yellow arrow head indicates double positive starter cells (GFP+ & HA+) in Figure 3. (**B, C**) Representative confocal microscopic images of coronal sections showing the neurons expressing FlpO fused with mCherry and HA tag in the PBN, related to the experiments in Figure 6 (B) and Figure7 (C). Yellow arrow head indicates double positive starter cells (mCherry-FlpO+ & HA+). Scale bars, 100 µm.

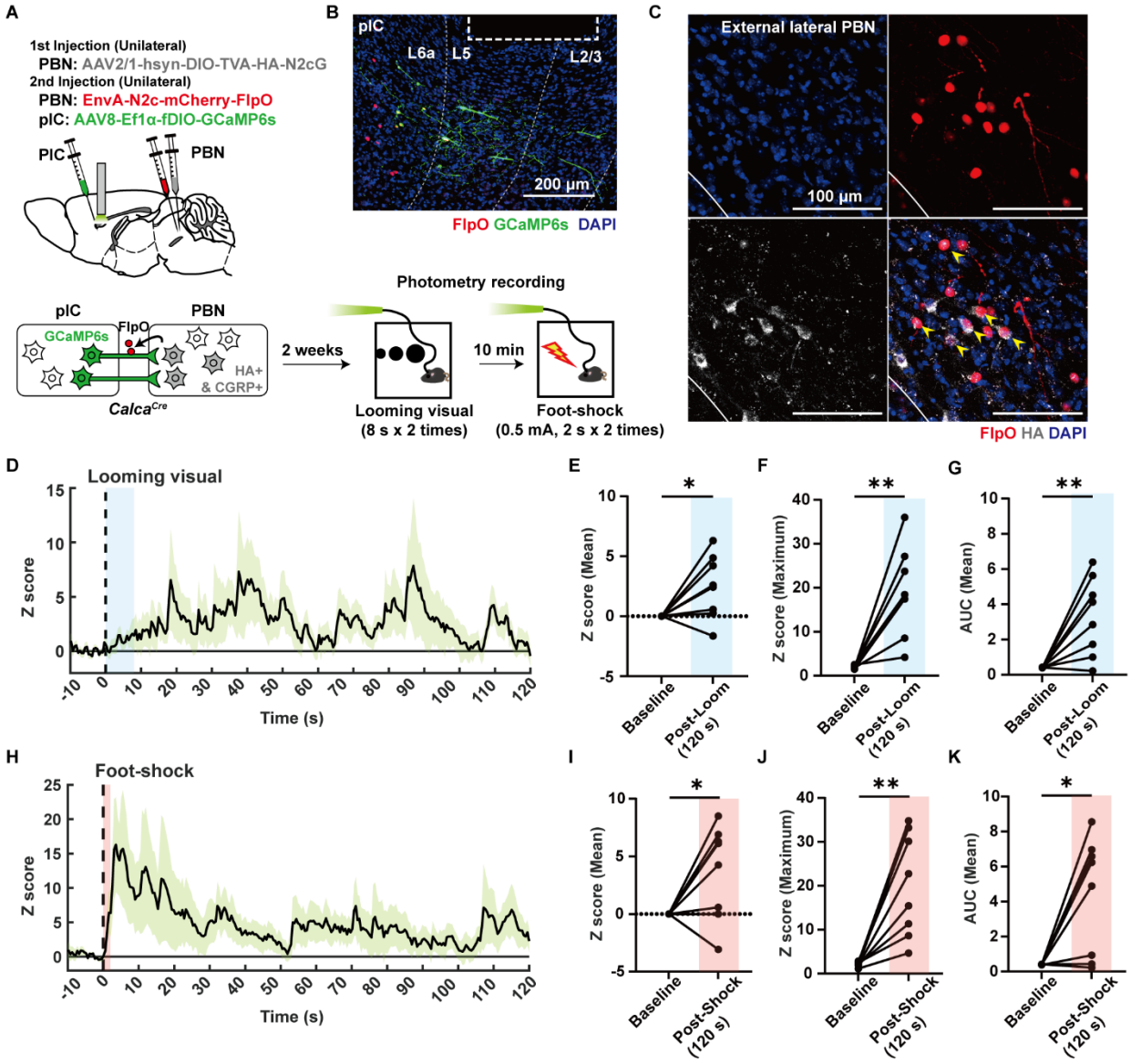
A
1st Injection (Unilateral)
PBN: AAV2/1-hsyn-DIO-TVA-HA-N2cG
2nd Injection (Unilateral)
PBN: EnvA-N2c-mCherry-FlpO
pIC: AAV8-Ef1α-fDIO-GCaMP6s
PIC
PBN
pIC
PBN
GCaMP6s
FlpO
HA+
& CGRP+
Calca^Cre
2 weeks
Photometry recording
10 min
Looming visual
(8 s x 2 times)
Foot-shock
(0.5 mA, 2 s x 2 times)
B
pIC
L6a
L5
L2/3
200 μm
FlpO GCaMP6s DAPI
C
External lateral PBN
100 μm
FlpO HA DAPI
D
Looming visual
Z score
Time (s)
E
Z score (Mean)
Baseline
Post-Loom (120 s)
F
Z score (Maximum)
G
AUC (Mean)
H
Foot-shock
I
Post-Shock (120 s)
J
K

1301

Fig. S6. CGRP^{PBN}-projecting pIC neurons (pIC$^{\rightarrow CGRP\text{-}PBN}$) respond to both looming and foot-shock stimuli (related to Figure 5).

(**A**) Schematic of fiber photometry recordings of responses of pIC$^{\rightarrow CGRP\text{-}PBN}$ neurons to looming and foot-shock stimuli. Unilateral injections of AAV2/1-hsyn-DIO-TVA-HA-N2cG into the PBN of *Calca*^{Cre} mice were followed by unilateral injections of EnvA-N2c-mCherry-FlpO into the same site, and unilateral injection of AAV8-Ef1α-fDIO-GCaMP6s and optic fiber implantation into the pIC. The stimuli were presented twice at a 120-s interval. (**B**) Representative confocal microscopic image of coronal section showing the neurons expressing GCaMP6s (green) and FlpO (red) in the pIC. All GCaMP6s+ cells were also FlpO+. The dotted rectangle indicates the location of optic fiber. Scale bar, 200 μm. (**C**) Representative confocal microscopic images of coronal sections showing the starter cells double positive for FlpO and HA tag in the PBN. Yellow arrowheads indicate double positive starter cells (FlpO-mCherry+ & HA+) in merged image. (**D**) Z-scored calcium activities (mean ± s.e.m) of pIC$^{\rightarrow CGRP\text{-}PBN}$ neurons in response to looming (baseline= -5 to 0s, Looming= 0-120 s after the onset of visual stimuli). Blue shaded area indicates a period (8 s) during which looming was presented. (**E-G**) Average Z score (E) ([N=8 trials (1 trial per mouse, 8 mice)]; one sample t-test, t_7= 2.615, P= 0.0347), maximum Z score (F) (two-tailed paired t-test, t_7= 4.787, P= 0.0020), and average AUC (G) (two-tailed paired t-test, t_7= 3.676, P= 0.0079) of calcium responses were measured. (**H**) Z-scored calcium activities (mean ± s.e.m) of pIC$^{\rightarrow CGRP\text{-}PBN}$ neurons in response to foot-shock (baseline= -5 to 0 s, Shock= 0-120 s after onset of foot-shock). Red shaded area indicates a period during which foot-shock (2 s) was presented. (**I-K**) Average Z score (I) (one sample t-test, t_7= 2.576, P= 0.0367), maximum Z score (J) (two-tailed paired t-test, t_7= 4.441, P= 0.0030), and average AUC (K) (two-tailed paired t-test, t_7= 3.358, P= 0.0121) of calcium responses were measured. All data are mean ± s.e.m. *p < 0.05. **p < 0.01. ns, not significant.